Original Article | Open Access

Metabolism and Target Organ Damage

Sun *et al. Metab Target Organ Damage.* 2026;6:69 **DOI:**10.20517/mtod.2026.162

Immune cell-resolved genetic associations nominate *FADS1* as a candidate locus in metabolic syndrome

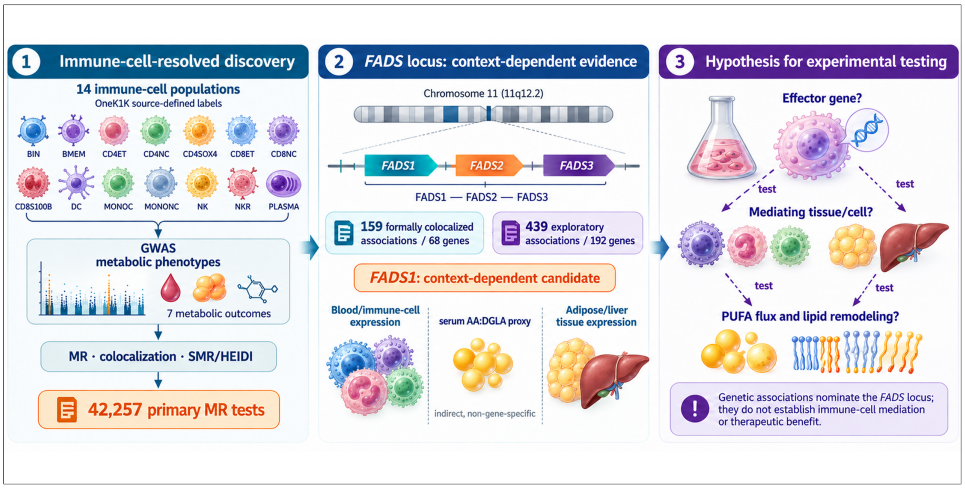
Yujing Sun[1,2,3,#], Xiaoli Zhang[1,2,#], Fuhua Zhang[1,4], Tianxin Yang[4], Siyue Li[1,4], Lina Wang[4], Xinxu Wang[1,4], Hui Wei[5], Qingwen Sun[6], Zhenhua Zhang[7], Xinguo Hou[1,2], Chuan Wang[1,2], Fuqiang Liu[1,2]

Keywords:
Metabolic syndrome, immune cell-specific eQTL, Mendelian randomization, *FADS1*, lipid metabolism, polyunsaturated fatty acids

Citation: Sun Y, Zhang X, Zhang F, Yang T, Li S, Wang L, Wang X, Wei H, Sun Q, Zhang Z, Hou X, Wang C, Liu F. Immune cell-resolved genetic associations nominate *FADS1* as a candidate locus in metabolic syndrome. *Metab Target Organ Damage.* 2026;6:69. https://dx.doi.org/10.20517/mtod.2026.162

Received: 23 Jul 2026 **First Decision:** 21 Sep 2026 **Revised:** 26 Oct 2026 **Accepted:** 27 Oct 2026 **Published:** 16 Nov 2026

Academic Editor: Amedeo Lonardo
Copy Editor: Ting-Ting Hu
Production Editor: Ting-Ting Hu



Abstract

Aim: To identify immune-cell-resolved genetic associations with metabolic syndrome (MetS) and prioritize candidate loci for further investigation.

Methods: We integrated cis-expression quantitative trait loci from 14 peripheral immune-cell populations with genome-wide association study summary statistics for two aggregate metabolic phenotypes and five component traits. We combined Mendelian randomization (MR), Bayesian colocalization, and summary-data-based Mendelian randomization (SMR) with heterogeneity in dependent instruments (HEIDI) testing. Transcriptomic and cross-sectional population analyses provided additional biological context.

Results: Among 42,257 primary MR tests, 3,141 gene-cell-trait associations met the prespecified false-discovery-rate threshold after outcome-specific correction. In a

[1]Department of Endocrinology and Metabolism, Qilu Hospital of Shandong University, Jinan 250012, Shandong, China.
[2]Shandong Provincial Key Laboratory of Spatiotemporal Regulation and Precision Intervention in Endocrine and Metabolic Diseases; Shandong Provincial Engineering Research Center for Advanced Technologies in Prevention and Treatment of Chronic Metabolic Diseases; Institute of Endocrine and Metabolic Diseases of Shandong University, Jinan 250012, Shandong, China.
[3]Department of Biochemistry and Molecular Biology, Mayo Clinic, Rochester, MN 55905, USA.
[4]The First Clinical Medical College, Cheeloo College of Medicine, Shandong University, Jinan 250012, Shandong, China.
[5]Rehabilitation Center, Qilu Hospital of Shandong University, Jinan 250012, Shandong, China.
[6]Department of Cardiology, Shandong Second Provincial General Hospital, Jinan 250012, Shandong, China.
[7]School of Pharmaceutical Sciences, Sun Yat-sen University, Guangzhou 510006, Guangdong, China.
[#]These authors contributed equally to this work and share first authorship.

Correspondence to: Prof. Chuan Wang, Prof. Fuqiang Liu, Department of Endocrinology and Metabolism, Qilu Hospital of Shandong University, Jinan 250012, Shandong, China. E-mail: wangchuan@email.sdu.edu.cn; liufuqiang@sdu.edu.cn

sensitivity analysis applying Benjamini-Hochberg correction across all 42,257 tests, 2,950 associations remained significant. Formal Bayesian colocalization supported 159 associations involving 68 genes. A broader exploratory pool contained 439 associations involving 192 genes, including 280 associations retained through a linkage disequilibrium (LD)-based screening criterion without formal colocalization support. Fatty acid desaturase 1 (*FADS1*) was prioritized as a candidate at the fatty acid desaturase (FADS) locus, which is associated with polyunsaturated fatty acid metabolism. Genetically proxied *FADS1* expression and the serum log-transformed ratio of arachidonic acid (AA) to dihomo-γ-linolenic acid (DGLA) showed differing metabolic association patterns; the AA/DGLA ratio represents an indirect and non-gene-specific biochemical proxy rather than a direct measure of FADS1 activity.

Conclusion: Immune-cell-resolved genetic analyses nominate the FADS locus and *FADS1* as candidates for further investigation, but do not establish the effector gene, mediating cell type, or lipid-remodeling mechanism. Direct functional and lipid measurements are needed to test these hypotheses.

INTRODUCTION

Metabolic syndrome (MetS) is a chronic inflammatory metabolic disorder characterized by central obesity, dyslipidemia, impaired glucose homeostasis, and hypertension, collectively contributing to increased risks of type 2 diabetes (T2D), cardiovascular disease, and premature mortality[1,2]. Beyond these clinical manifestations, growing evidence indicates that MetS is fundamentally driven by chronic low-grade inflammation and widespread immunometabolic dysfunction[3,4]. Immune cells actively participate in adipose tissue remodeling, lipid handling, inflammatory cytokine production, and systemic metabolic regulation, thereby contributing to the progression of obesity-associated metabolic and cardiovascular complications[5,6]. Although single-cell expression quantitative trait locus (eQTL) studies have identified immune-cell-resolved regulatory effects and their relevance to disease susceptibility[7], the contribution of genetically regulated gene expression in specific immune-cell populations to MetS remains insufficiently characterized.

Genome-wide association studies (GWAS) have identified numerous susceptibility loci associated with obesity, dyslipidemia, insulin resistance, and related cardiometabolic traits[8,9]. However, translating disease-associated loci into biological mechanisms remains challenging because genetic effects on gene expression can depend on the cellular state in which they are measured[10]. In particular, bulk-tissue expression analyses average signals across heterogeneous cell populations and may obscure cell-type-dependent genetic regulatory effects[11]. Recent advances in single-cell transcriptomics and cell-type-resolved eQTL mapping now enable characterization of genetically regulated transcriptional programs at immune-cell resolution, providing new opportunities to investigate lineage-specific immunometabolic regulation[12].

Lipid remodeling represents another central component of MetS pathophysiology. In particular, polyunsaturated fatty acid (PUFA) metabolism influences membrane composition, lipid mediator synthesis, inflammatory signaling, and cardiometabolic homeostasis. Fatty acid desaturase 1 (*FADS1*) is of particular interest because it encodes the rate-limiting Δ5-desaturase involved in PUFA remodeling. *FADS1* has consistently been associated with circulating lipid profiles, inflammatory responses, obesity-related phenotypes, and cardiovascular-metabolic risk[13]. Moreover, emerging nutrigenetic evidence suggests that dietary PUFA exposure may modify the metabolic effects of *FADS1* genetic variation, highlighting a potential biological interface linking diet, lipid remodeling, inflammation, and metabolic dysfunction[14,15]. Nevertheless, how immune cell-specific genetic regulation intersects with lipid remodeling and dietary fatty acid-related metabolic risk remains insufficiently understood. To address these gaps, the present study aimed to characterize the immune cell-resolved genetic architecture of MetS and its related metabolic traits. We

sought to identify immune cell-specific genetically regulated genes associated with metabolic phenotypes and to prioritize candidate regulators linking immune function, lipid remodeling, inflammation, and metabolic risk. This framework was designed to provide mechanistic insight into immune-metabolic regulation and to support the discovery of candidate molecular axes relevant to MetS.

METHODS

Study design and overall analytical framework

This study used an integrative genetic prioritization framework to evaluate whether genetically regulated gene expression in peripheral immune-cell subsets was associated with MetS and related metabolic traits. The primary genetic evidence comprised immune-cell-specific Mendelian randomization (MR), regional colocalization, and summary-data-based Mendelian randomization (SMR) with heterogeneity in dependent instruments (HEIDI) testing. Blood eQTL data from the eQTLGen consortium and tissue-specific eQTL data from the Genotype-Tissue Expression (GTEx) project were used for cross-platform validation. Downstream functional enrichment, protein-protein interaction (PPI) network analysis, cross-tissue transcriptomic analysis, population-level fatty acid analysis, compound-target annotation, and molecular docking were used for candidate prioritization. The observational and *in silico* analyses were considered supportive and hypothesis-generating and were not interpreted as experimental evidence of therapeutic efficacy.

This study involved secondary analyses of publicly available summary-level genetic data and de-identified individual-level data. No new human participants were recruited and no additional human specimens were collected. The original studies obtained the relevant ethical approvals and informed consent. Therefore, no additional ethical approval or informed consent was required for the present secondary analysis.

Single-cell cis-eQTL datasets and immune cell annotation

Single-cell cis-eQTL summary statistics were obtained from the OneK1K study[7], which profiled peripheral blood mononuclear cells (PBMCs) from 982 individuals of European ancestry. Fourteen immune-cell populations were included, comprising naïve and memory B cells, plasma cells, $CD4^+$ and $CD8^+$ T-cell subsets, natural killer cells, dendritic cells, and classical and non-classical monocytes. Cell type-specific effective sample sizes are reported in Supplementary Table 1A.

Cis-eQTLs associated with gene expression at $P < 5 \times 10^{-8}$ were considered candidate instruments. The numbers of eQTLs before and after linkage-disequilibrium clumping are summarized in Supplementary Table 1B. The distribution of genes by the number of instrumental variants is presented in Supplementary Table 1C. For MR, effect alleles were harmonized between the exposure and outcome datasets before estimation. Complete variant-level information, including chromosome, genomic position, effect and non-effect alleles, effect-allele frequency, association estimates, sample size, variance explained, and *F*-statistics, is provided in Supplementary Table 1D.

GWAS datasets for metabolic traits

Summary statistics were obtained for two aggregate metabolic phenotypes - a common genetic factor for MetS and the FinnGen release 12 metabolic-disorders endpoint - and five component traits: waist circumference, hypertension, fasting glucose, triglycerides, and high-density lipoprotein cholesterol. Thus, seven outcome datasets were included in the analyses. All datasets were derived from populations of predominantly European ancestry to match the ancestry of the single-cell eQTL reference panel and reduce confounding due to population structure. Dataset sources, accession identifiers, phenotype definitions, study designs or trait scales, sample sizes, and ancestry information are provided in Supplementary Table 2.

Mendelian randomization and causal inference analyses

Genome-wide significant cis-eQTLs were selected at $P < 5 \times 10^{-8}$ and clumped using an r^2 threshold of 0.001 within a 10,000-kb window. Instrument strength was evaluated using the proportion of exposure variance explained and the *F* statistic, calculated as $F = R^2(N - 2)/(1 - R^2)$. Instruments with $F > 10$ were considered sufficiently strong.

For exposure-outcome pairs with one genetic instrument, the Wald ratio was used as the primary estimator. For pairs with two or more instruments, inverse-variance weighting was used as the primary estimator. For three-instrument analyses, MR-Egger regression, weighted-median, simple-mode, and weighted-mode estimates were reported as secondary analyses. *P* values from the primary estimator were adjusted using the Benjamini-Hochberg procedure separately within each outcome. Complete primary and secondary MR estimates are provided in Supplementary Table 3.

Cochran Q statistics were used to evaluate heterogeneity when at least two instruments were available. The MR-Egger intercept was used to assess directional horizontal pleiotropy for three-instrument analyses. Steiger tests were performed for all primary analyses to assess whether the genetic instruments explained more variance in the exposure than in the outcome. Mendelian randomization pleiotropy residual sum and outlier (MR-PRESSO) was prespecified for analyses with at least four instruments; however, because no exposure-outcome analysis contained more than three instruments, MR-PRESSO outlier and distortion tests were not applicable. Because most exposure-outcome pairs were instrumented by a single variant, the Wald-ratio estimates could not be evaluated using multi-instrument pleiotropy diagnostics; instrument strength and Steiger tests do not exclude horizontal pleiotropy. Complete heterogeneity, horizontal pleiotropy, Steiger directionality, and other sensitivity analysis results are provided in Supplementary Table 4.

Regional colocalization analyses

Regional colocalization was first evaluated using the approximate Bayes factor framework implemented in the coloc package. Prior probabilities were set to $p1 = 1 \times 10^{-4}$, $p2 = 1 \times 10^{-4}$, and $p12 = 1 \times 10^{-5}$. Posterior probabilities were reported for no association with either trait, association with the expression trait only, association with the metabolic outcome only, two distinct causal variants, and a shared causal variant (PP.H0-PP.H4). Formal approximate Bayes factor colocalization support was defined as raw PP.H4 ≥ 0.70. The conditional quantity PP.H4/(PP.H3 + PP.H4) was reported as a diagnostic measure but was not used as the formal colocalization criterion.

Regions with PP.H3 ≥ 0.50 were further evaluated using sum of single effects (SuSiE)-based colocalization to allow for multiple causal signals. Expression and outcome summary statistics were aligned to the alleles and variant order of the 1,000 Genomes European linkage disequilibrium (LD) reference panel before model fitting. SuSiE was run with L = 3, scaled_prior_variance = 0.01, estimate_prior_variance = FALSE, a maximum of 1,000 iterations, and a convergence tolerance of 1×10^{-3}. Quantitative outcomes were specified as quantitative traits, whereas binary outcomes were specified as case-control traits with the corresponding case fraction. Formal SuSiE support was defined as PP.H4 ≥ 0.70. All evaluated signal pairs, posterior probabilities, numbers of overlapping single-nucleotide polymorphisms (SNPs), convergence status, and failure reasons are provided in Supplementary Table 5. Colocalization was interpreted as evidence compatible with a shared regional signal, rather than identification of a unique effector gene or mediating cell type. This distinction is particularly relevant to linked loci such as the *FADS1-FADS2-FADS3* region.

Evidence classification. Associations meeting the prespecified PP.H4 ≥ 0.70 criterion in the approximate Bayes factor or SuSiE analysis were classified as formally colocalized. An additional 280 associations had been retained through an exploratory LD-based mapping procedure. Because this procedure did not apply a

prespecified LD threshold and did not constitute a statistical colocalization test, these associations were classified separately as exploratory LD-screened signals. They were not included in the formally colocalized set or interpreted as evidence of a shared causal variant. The variant pairs, LD values, reference panel, and analysis status for this exploratory screen are reported in Supplementary Table 5D.

Summary-data-based Mendelian randomization and HEIDI analysis

SMR was performed to evaluate associations between genetically predicted gene expression and metabolic outcomes. The HEIDI test was used to assess whether each SMR association was compatible with a shared causal variant rather than linkage between distinct causal variants. SMR *P* values were adjusted using the Benjamini-Hochberg procedure. Associations were considered statistically supported when the SMR false discovery rate (FDR) was < 0.05 and the HEIDI *P* value was greater than 0.05. Complete results, including probe identifier, top eQTL, expression and outcome association estimates, SMR effect estimate, standard error, nominal and adjusted *P* values, HEIDI *P* value, number of SNPs used in HEIDI, and analysis status, are provided in Supplementary Table 6.

Cross-platform validation using eQTLGen and GTEx

Blood eQTL summary statistics from the eQTLGen consortium were used for two-sample MR validation. The Wald ratio was used for one-instrument analyses, whereas inverse-variance weighting was used for analyses with two or more instruments; secondary MR estimators were reported separately when applicable. Complete eQTLGen validation results are provided in Supplementary Table 7.

Tissue-specific eQTL data from 49 tissues in the GTEx project were integrated with the metabolic-outcome GWAS datasets using SMR and HEIDI analyses. The same significance and HEIDI criteria used in the primary analyses were applied. Complete GTEx SMR and HEIDI results are provided in Supplementary Table 8.

For cross-platform validation, all gene-trait pairs with available effect estimates in both the discovery and corresponding validation datasets were included. Sign concordance was defined as agreement in the direction of the effect estimate between the discovery analysis and the validation dataset. The sign-concordance rate was calculated as the number of overlapping pairs with concordant effect directions divided by the total number of overlapping pairs with available estimates. Nominal replication was defined as a concordant validation association meeting the prespecified nominal significance threshold ($P < 0.05$). Sign-concordance rates and nominal replication fractions were calculated separately for eQTLGen and GTEx and are reported in Supplementary Tables 7 and 8, respectively.

Functional enrichment and network analyses

Genes identified through MR analyses were subjected to functional enrichment analysis using curated biological pathway databases, including Gene Ontology (GO) and Kyoto Encyclopedia of Genes and Genomes (KEGG). Over-representation analysis was conducted to identify biological processes and pathways enriched among MR-prioritized candidate genes.

PPI networks were constructed using high-confidence interaction data from publicly available PPI databases. Network topology and modular structure were analyzed using the Molecular Complex Detection (MCODE) algorithm to identify densely connected gene clusters. Identified modules were interpreted as functional units underlying coordinated immunometabolic regulation.

Multi-layer gene prioritization

Candidate genes were prioritized using five prespecified score components: (1) recurrence of primary MR support across the predefined mapping groups; (2) pathway-enrichment evidence; (3) membership in prioritized MCODE modules; (4) PPI network connectivity; and (5) druggability evidence based on known compound-target annotations. The composite priority score was calculated as the sum of the MR recurrence, pathway, MCODE, PPI, and druggability component scores. Genes were classified as Tier 1 (total score ≥ 1.00), Tier 2 (≥ 0.35, < 1.00), or Tier 3 (< 0.35).

Formal Bayesian colocalization and SMR/HEIDI analyses were treated as independent validation evidence rather than components of the composite priority score. In particular, a non-significant HEIDI test was interpreted as being more consistent with a shared causal variant, whereas a significant test suggested heterogeneity potentially attributable to linkage. Associations identified only by the exploratory linkage-disequilibrium-based screen were retained as exploratory candidates and were not described as formally colocalized or causally validated.

Cross-tissue transcriptomic analyses

Independent transcriptomic datasets from PBMCs, monocytes, liver tissue, adipose tissue, and skeletal muscle were analyzed to evaluate disease-associated expression patterns of prioritized genes. Public datasets included GSE200744, GSE32575, GSE196387, GSE159924, GSE126848, GSE141432, and GSE24883. Differential expression analyses were conducted using normalized expression matrices and compared across metabolic disease states including obesity, MetS, non-alcoholic fatty liver disease (NAFLD), non-alcoholic steatohepatitis (NASH), and T2D.

NHANES analyses

Population-level cross-sectional analyses were conducted using data from the 2013-2014 National Health and Nutrition Examination Survey (NHANES). The following files were linked using the participant identifier SEQN: DEMO_H for demographic and survey-design variables; DR1TOT_H for first-day dietary intake and total energy intake; FAS_H for serum fatty acid concentrations and the fatty acid subsample weight; BMX_H for body mass index and waist circumference; GHB_H for glycated hemoglobin; GLU_H for fasting glucose; TCHOL_H, HDL_H, and TRIGLY_H for total cholesterol, high-density lipoprotein cholesterol, triglycerides, and low-density lipoprotein cholesterol; BPX_H for systolic and diastolic blood pressure; and CBC_H for white blood cell and differential blood-cell counts, including neutrophil counts. Derived variables, including non-HDL cholesterol, the triglycerides/high-density lipoprotein cholesterol (TG/HDL-C) ratio, and neutrophil-to-lymphocyte and monocyte-to-lymphocyte ratios, were calculated after merging the component files.

Adults aged ≥ 20 years were eligible if they had valid fatty acid subsample weights, survey-design variables, first-day total energy intake, dietary fatty acid intake data, and arachidonic acid (AA) and dihomo-γ-linolenic acid (DGLA) concentrations. Participants with non-positive AA or DGLA concentrations, non-positive total energy intake, or missing prespecified covariates were excluded.

The log-transformed AA/DGLA ratio was used as an indirect biochemical proxy of Δ5-desaturase activity and was not interpreted as a direct measurement of FADS1 activity. Because AA and DGLA are mathematical components of this ratio, analyses of individual circulating fatty acids were treated as supportive descriptive analyses and were reported separately from the ratio-based analyses.

Dietary linoleic acid (LA), α-linolenic acid (ALA), eicosapentaenoic acid (EPA), and docosahexaenoic acid (DHA) intakes were obtained from the first 24-h dietary recall using DR1TP182, DR1TP183, DR1TP205, and DR1TP226, respectively. Dietary EPA and DHA were also summed to derive a combined EPA + DHA

exposure. The dietary LA/(ALA + EPA + DHA) ratio was calculated as DR1TP182/(DR1TP183 + DR1TP205 + DR1TP226) before log transformation and standardization. All dietary fatty acid intakes were expressed in grams per day. This ratio represents the balance of the selected dietary fatty acids and should not be interpreted as a comprehensive ratio of total dietary n-6 to total dietary n-3 fatty acids. Participants with missing component values or a non-positive denominator were excluded from the ratio-specific analysis.

Dietary LA and ALA were transformed using ln(intake + 0.01), whereas EPA, DHA, and combined EPA + DHA were transformed using ln(intake + 0.001). The dietary ratio was transformed using ln(ratio + 0.01). The transformed dietary exposures were standardized to standard-deviation units before modeling. The log-transformed AA/DGLA ratio was used as the outcome in the dietary-exposure analyses.

Survey-weighted linear regression models were fitted using NHANES strata, primary sampling units, and the serum fatty acid subsample weight (WTFAS2YR). Models were adjusted for age, sex, self-reported race and ethnicity, and standardized total energy intake. Dietary LA, ALA, EPA, DHA, EPA + DHA, and the LA/(ALA + EPA + DHA) ratio were each evaluated in separate models. Nominal *P* values, 95% confidence intervals, and Benjamini-Hochberg-adjusted *P* values were reported for this six-exposure testing family.

Associations between the log-transformed AA/DGLA proxy and cardiometabolic traits were estimated separately using survey-weighted models with the same sampling design. These models were adjusted for age, sex, race and ethnicity, and other prespecified covariates as appropriate for each outcome. Benjamini-Hochberg correction was applied within each prespecified cardiometabolic outcome domain.

Molecular docking and virtual screening

The three-dimensional structure of human FADS1 (UniProt accession O60427) was obtained from the AlphaFold Protein Structure Database (model AF-O60427-F1). The receptor structure was prepared using AutoDockTools by removing water and other non-essential molecules, adding polar hydrogen atoms, assigning Gasteiger charges, and converting the structure to PDBQT format. A library of 5,903 approved or investigational small molecules was obtained from the "world" subset of the ZINC15 database (https://zinc15.docking.org/substances/subsets/world). Ligand structures in MOL2 format were converted to PDBQT format using MGLTools. The complete compound source and preparation information are provided in Supplementary Table 9. Molecular docking was performed using AutoDock Vina with a grid centered at x = 1, y = -8, and z = 0 Å and dimensions of 35 $Å^3$ × 30 $Å^3$ × 34 $Å^3$. Exhaustiveness was set to 30, up to nine binding modes per ligand were retained, and the energy range was set to 3 kcal/mol. Compounds were ranked according to their lowest predicted binding energy. The displayed compounds do not represent the complete ranked output of the 5,903-compound screen. Selected docking poses were visualized using PyMOL and LigPlot+. Docking results were interpreted as hypothesis-generating evidence of structural compatibility only and were not considered evidence of biochemical binding, target engagement, pharmacological efficacy, safety, or therapeutic tractability.

Statistical analysis

Statistical analyses were performed using R version 4.5.1. All tests were two-sided. For the primary MR analysis, Benjamini-Hochberg correction was performed separately within each metabolic outcome using one prespecified primary estimator per exposure-outcome pair. Each gene-cell exposure was treated as a separate test within its outcome, so the outcome-specific correction included tests across the 14 immune-cell contexts. To assess multiplicity across outcomes, we additionally applied the Benjamini-Hochberg procedure to all 42,257 primary MR tests as one family. This pooled analysis was reported as a sensitivity analysis; downstream candidate selection in the original workflow used outcome-specific FDR values. Secondary MR estimators were reported as sensitivity analyses and were not used to define the primary significant set.

Approximate Bayes factor and SuSiE colocalization were evaluated using posterior-probability thresholds rather than FDR correction. SMR *P* values were adjusted using the Benjamini-Hochberg procedure separately within each metabolic outcome across all evaluated probes. HEIDI results were interpreted using a prespecified threshold of $P > 0.05$. NHANES models incorporated the survey weights, strata, and primary sampling units; multiple-testing correction was performed within prespecified cardiometabolic outcome domains. Exact *P* values, confidence intervals, denominators, and numbers of evaluable analyses are reported in the corresponding supplementary tables.

RESULTS

Immune cell-specific distribution of eQTLs reveals lineage-dependent genetic regulation

To characterize the distribution of genetic instruments across immune-cell subsets, we curated 1,970,799 genome-wide significant cis-eQTL records ($P < 5 \times 10^{-8}$), involving 3,335 genes across 14 immune-cell subsets. LD clumping at $r^2 < 0.001$ within a 10,000-kb window retained 9,117 independent cis-eQTL instruments representing 3,319 genes for downstream MR analyses [Figure 1A and B, Supplementary Table 1]. All retained instruments had *F*-statistics greater than 10, with a minimum *F* statistic of 29.66, indicating adequate instrument strength.

Figure 1C summarizes the sample size of each immune-cell eQTL panel, whereas Figure 1D and E show the numbers of cell-specific eGenes supported by one, two, or three independent instruments. The distribution of retained instruments varied across immune-cell subsets. CD4-positive naïve/central-memory T cells accounted for approximately 25.8% of the retained instruments, whereas CD4-positive SOX4-expressing T cells and dendritic cells contributed smaller proportions. These differences describe the availability and distribution of genetic instruments across immune-cell subsets and should not be interpreted as evidence that one cell type has stronger causal effects or greater biological importance than another.

Identification of immune-cell-specific Mendelian-randomization-prioritized associations for metabolic syndrome and its components

To identify immune-cell-specific gene-expression associations with MetS and its component traits, we performed two-sample MR using single-cell cis-eQTLs from 14 peripheral-blood immune-cell subsets [Figure 2]. Using 9,117 independent cis-eQTL instruments, we conducted 42,257 primary gene-cell-trait tests, comprising 40,849 Wald-ratio estimates based on a single instrument and 1,408 inverse-variance-weighted estimates based on two or more instruments. Instrument strength was adequate, with a minimum *F* statistic of 29.66. Steiger tests favored the specified exposure-to-outcome orientation for all 42,257 primary tests; this result was treated as a consistency check rather than proof of causal direction. After the outcome-specific Benjamini-Hochberg correction, 3,141 associations remained significant at FDR < 0.05, including 3,067 Wald-ratio and 74 inverse-variance-weighted estimates [Supplementary Tables 1-4]. These 3,141 association records involved 2,322 distinct gene-cell exposures across the seven outcomes. In a sensitivity analysis correcting across all 42,257 primary tests, 2,950 records involving 2,150 distinct exposures met FDR < 0.05. These findings were interpreted as MR-prioritized associations rather than definitive evidence of causality.

Among the FDR-significant results, 2,643 gene-cell-trait association records involved the five metabolic-syndrome component traits: triglycerides (TG), high-density lipoprotein cholesterol (HDL-C), fasting glucose (FG), waist circumference (WC), and hypertension (HTN) [Supplementary Table 10A]. After deduplication by immune-cell-specific gene exposure - that is, a gene-cell pair - these records represented 2,210 unique gene-cell exposures [Supplementary Table 10B]. Figure 2A summarizes the overlap of these exposures across the five component traits. No exposure was shared across all five traits, although partial overlaps were observed between subsets of traits. These patterns indicate partial sharing of

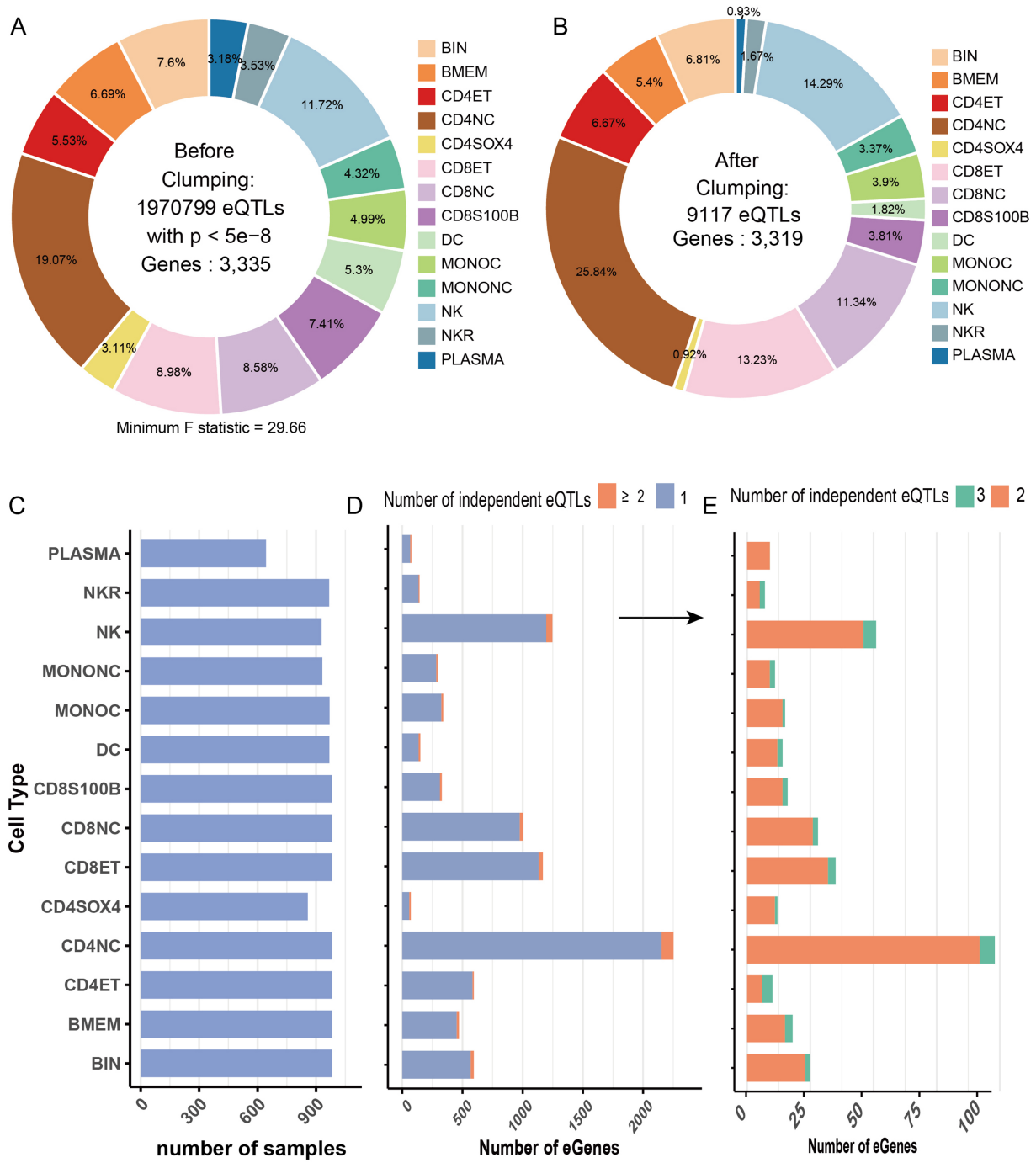


Figure 1. Selection and distribution of immune cell-specific cis-eQTL instruments for Mendelian randomization analysis. (A) Proportional distribution of 1,970,799 genome-wide-significant cis-eQTL association records ($P < 5 \times 10^{-8}$) across 14 immune-cell populations before linkage disequilibrium clumping. These records corresponded to 3,335 unique genes in the OneK1K peripheral-blood mononuclear-cell dataset; (B) Distribution of retained instrument records across immune-cell populations after gene- and cell-type-specific LD clumping. The number of unique genes decreased from 3,335 before clumping to 3,319 after clumping. Clumping was performed using $r^2 < 0.001$ within a 10,000-kb window. This intentionally broad window was used to minimize the retention of correlated cis-instruments across extended regulatory regions. A total of 9,117 cell-type-specific cis-eQTL instrument records, representing 8,733 gene-cell exposures and 3,319 unique genes, were retained for downstream analyses. The minimum *F* statistic among the retained instruments was 29.66. Because the same genetic variant could serve as an instrument for more than one gene or immune-cell context, the 9,117 instrument records corresponded to 6,776 unique variant identifiers; (C) Cell-type-specific donor sample sizes in the OneK1K single-cell eQTL dataset; (D) Number of cell-type-specific eQTL-associated genes, grouped according to whether their expression was instrumented by exactly one or by two or more independent cis-eQTLs. A gene represented in more than one immune-cell population was counted separately in each corresponding gene-cell context; (E) Expanded view of the multi-instrument group shown in panel D, separating gene-cell exposures supported by exactly two or exactly three independent cis-eQTL instruments. No evaluated gene-cell exposure contained more than three independent instruments. Source data and cell-type-specific donor sample sizes are provided in Supplementary Table 1A, and complete instrument-level information is provided in Supplementary Table 1D. BIN: Naïve/immature B cells; BMEM: memory B cells; CD4ET: $CD4^+$ effector-memory/TEMRA T cells; CD4NC: $CD4^+$ naïve/central-memory T cells; CD4SOX4: $CD4^+$ SOX4-expressing T cells; CD8ET: $CD8^+$ effector-memory T cells; CD8NC: $CD8^+$ naïve/central-memory T cells; CD8S100B: $CD8^+$ S100B-expressing T cells; DC: dendritic cells;

eQTL: expression quantitative trait locus; LD: linkage disequilibrium; MONOC: classical monocytes; MONONC: non-classical monocytes; NK: natural killer cells; NKR: natural killer recruiting cells; PLASMA: plasma cells; TEMRA: terminally differentiated effector memory T cells re-expressing CD45RA.

immune-cell-specific genetic associations together with substantial trait specificity. The requirement for association with at least three of five component traits was an exploratory selection rule used to reduce the number of component-trait regions entering regional mapping. It was not applied to the single-outcome CTG or FinnGen branches; consequently, counts and overlap across these branches should not be interpreted as a comparison of recurrence under equivalent selection rules.

Figure 2B summarizes the branch-specific screening process at the gene-cell-exposure level. The Complex Trait Genetics (CTG) Lab and FinnGen analyses yielded 364 and 134 FDR-significant gene-cell exposures, respectively. For the five component traits, the 163 gene-cell-trait records included in the regional analysis corresponded to 54 deduplicated gene-cell exposures [Supplementary Table 5A]. To assess sensitivity to this exploratory carry-forward threshold, we also counted exposures meeting alternative recurrence cutoffs under the same outcome-specific FDR screen. Requiring associations with at least two, three, or four of the five component traits yielded 378, 54, and 1 gene-cell exposures, respectively. These alternative counts describe eligibility under each cutoff; regional mapping was performed using the original ≥ 3-of-5 rule. Application of the legacy broad shared-signal rule retained 203 exposures in the CTG analysis, 123 in the FinnGen analysis, and 53 among the component traits. This broad rule combined formal Bayesian colocalization support with an exploratory linkage-disequilibrium-based criterion; consequently, these counts should not be interpreted as representing formal Bayesian colocalization alone.

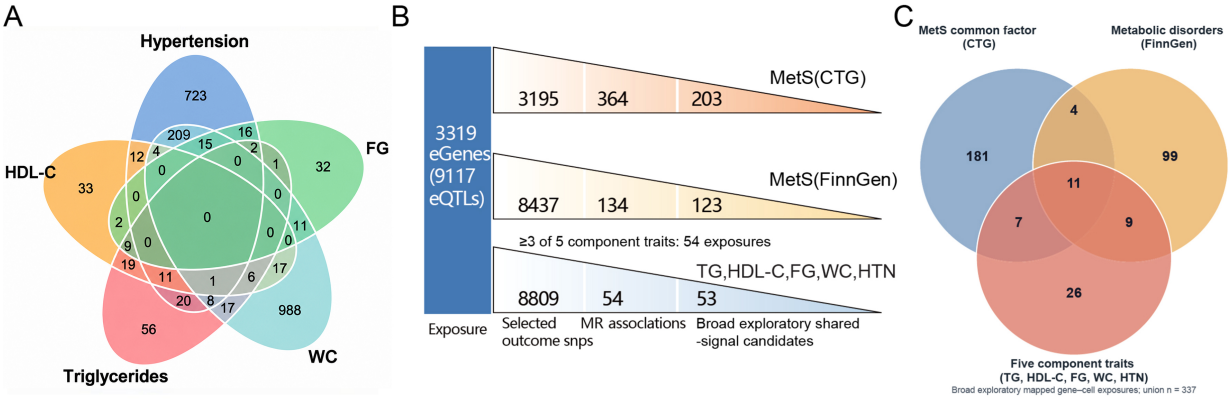
At the gene-cell-exposure level, the three broad sets comprised 337 distinct exposures, including 181 unique to CTG, 99 unique to FinnGen, and 26 unique to the component-trait group [Figure 2C]. Thirty-one exposures were represented in at least two mapping groups, of which 11 were shared across all three groups. This overlap indicates partial convergence across outcome datasets but does not by itself establish independent replication or causality.

Figure 2D presents selected immune-cell-specific MR estimates involving *FADS1*, *TMEM258*, *ABHD16A*, *HSPA1L*, and *LY6G5B*. For binary outcomes, exponentiated estimates can be interpreted as odds ratios with 95% confidence intervals. For continuous outcomes, beta coefficients remain the primary effect measures. The *FADS1*-annotated estimates shown in Figure 2D are based on genetic instruments for expression in the indicated immune-cell populations. They do not establish that *FADS1*, rather than another gene at the linked FADS locus, mediates the metabolic association, or that the profiled immune cell is the causal tissue.

Mapping trait-gene-cell specificity reveals immunometabolic pleiotropy and modularity

To further understand the structural logic of immune regulation across metabolic traits, we mapped the cross-trait and cross-cell-type patterns of the 28 pleiotropic MR-prioritized candidate genes [Figure 3 and Supplementary Table 10]. The Circos plot [Figure 3A] illustrates how these genes connect to three broad trait categories: MetS (CTG), MetS (FinnGen), and aggregated metabolic components [TG, HDL-C, FG, WC, and HTN]. Genes like *FADS1*, *HSPA1L*, and *TMEM258* displayed extensive trait and cell connectivity, supporting their central roles in immunometabolic regulation.

The bubble plot [Figure 3B] shows the number of detected trait associations for each gene across the profiled immune-cell populations. $CD4^+$ effector T cells, memory B cells, and non-classical monocytes had more associations in the displayed set. The accompanying bar charts summarize the distribution of these associations across cells and phenotype groups. The heatmap and dendrogram [Figure 3C] group cell



D

Gene	Cell type	Outcome	β	SE	P value	β (95% CI)	BH FDR
ABHD16A	CD4ET	MetS (CTG)	0.028	0.006	1.16×10^{-5}	0.028 (0.016–0.041)	3.69×10^{-4}
ABHD16A	MONONC	MetS (CTG)	0.024	0.005	2.51×10^{-6}	0.024 (0.014–0.034)	9.99×10^{-5}
FADS1	BMEM	MetS (CTG)	0.012	0.004	2.62×10^{-3}	0.012 (0.004–0.020)	2.95×10^{-2}
FADS1	CD8NC	MetS (CTG)	-0.024	0.007	4.43×10^{-4}	-0.024 (-0.038–-0.011)	7.74×10^{-3}
FADS1	NK	MetS (CTG)	0.045	0.007	1.09×10^{-9}	0.045 (0.030–0.059)	1.22×10^{-7}
FADS1	CD4ET	MetS (CTG)	0.032	0.005	4.88×10^{-10}	0.032 (0.022–0.042)	5.69×10^{-8}
HSPA1L	CD8S100B	MetS (CTG)	-0.017	0.004	1.05×10^{-4}	-0.017 (-0.026–-0.009)	2.29×10^{-3}
LY6G5B	NK	MetS (CTG)	-0.030	0.007	2.80×10^{-5}	-0.030 (-0.045–-0.016)	7.28×10^{-4}
TMEM258	CD4NC	MetS (CTG)	0.018	0.003	2.63×10^{-8}	0.018 (0.012–0.025)	2.37×10^{-6}
TMEM258	BIN	MetS (CTG)	0.039	0.007	2.63×10^{-8}	0.039 (0.025–0.053)	2.37×10^{-6}
TMEM258	CD4ET	MetS (CTG)	0.033	0.006	2.63×10^{-8}	0.033 (0.021–0.044)	2.37×10^{-6}
FADS1	CD8NC	FG	-0.034	0.006	2.72×10^{-9}	-0.034 (-0.045–-0.023)	1.35×10^{-6}
FADS1	BMEM	FG	0.020	0.003	7.37×10^{-10}	0.020 (0.014–0.027)	4.13×10^{-7}
FADS1	NK	FG	-0.056	0.006	1.02×10^{-18}	-0.056 (-0.069–-0.044)	2.13×10^{-15}
FADS1	CD4ET	FG	0.041	0.004	4.88×10^{-20}	0.041 (0.032–0.050)	1.37×10^{-16}
TMEM258	BIN	FG	-0.047	0.006	7.38×10^{-15}	-0.047 (-0.059–-0.035)	5.17×10^{-12}
TMEM258	CD4NC	FG	-0.022	0.003	7.38×10^{-15}	-0.022 (-0.028–-0.017)	5.17×10^{-12}
TMEM258	CD4ET	FG	-0.040	0.005	7.38×10^{-15}	-0.040 (-0.050–-0.030)	5.17×10^{-12}
FADS1	BMEM	HDL-C	0.051	0.007	1.98×10^{-13}	0.051 (0.038–0.065)	4.06×10^{-11}
FADS1	CD8NC	HDL-C	-0.100	0.012	8.43×10^{-17}	-0.100 (-0.124–-0.077)	2.68×10^{-14}
FADS1	NK	HDL-C	-0.126	0.013	2.67×10^{-23}	-0.126 (-0.151–-0.101)	1.91×10^{-20}
FADS1	CD4ET	HDL-C	0.092	0.009	2.00×10^{-23}	0.092 (0.074–0.110)	1.91×10^{-20}
TMEM258	BIN	HDL-C	-0.112	0.012	2.89×10^{-19}	-0.112 (-0.136–-0.088)	1.18×10^{-16}
TMEM258	CD4ET	HDL-C	-0.094	0.010	2.89×10^{-19}	-0.094 (-0.115–-0.073)	1.18×10^{-16}
TMEM258	CD4NC	HDL-C	-0.052	0.006	2.89×10^{-19}	-0.052 (-0.064–-0.041)	1.18×10^{-16}

Quantitative outcomes — β coefficients (95% CI); null = 0

−0.15 −0.10 −0.05 0.00 0.05 0.10

β coefficient

Binary outcomes — FinnGen metabolic disorders and hypertension; odds ratios (95% CI); null = 1

Gene	Cell type	Outcome	log(OR)	SE	P value	OR (95% CI)	BH FDR
ABHD16A	MONONC	Metabolic disorders (FinnGen)	0.055	0.013	4.46×10^{-5}	1.056 (1.029–1.085)	4.76×10^{-3}
ABHD16A	CD4ET	Metabolic disorders (FinnGen)	0.110	0.016	1.22×10^{-11}	1.116 (1.081–1.152)	7.64×10^{-9}
FADS1	CD8NC	Metabolic disorders (FinnGen)	-0.075	0.021	3.60×10^{-4}	0.927 (0.890–0.967)	2.48×10^{-2}
FADS1	BMEM	Metabolic disorders (FinnGen)	0.043	0.012	3.06×10^{-4}	1.044 (1.020–1.069)	2.18×10^{-2}
FADS1	CD4ET	Metabolic disorders (FinnGen)	0.059	0.015	4.37×10^{-5}	1.061 (1.031–1.092)	4.73×10^{-3}
FADS1	NK	Metabolic disorders (FinnGen)	-0.085	0.021	3.75×10^{-5}	0.919 (0.882–0.956)	4.29×10^{-3}
HSPA1L	CD8S100B	Metabolic disorders (FinnGen)	-0.098	0.014	6.11×10^{-12}	0.907 (0.882–0.933)	4.96×10^{-9}
LY6G5B	NK	Metabolic disorders (FinnGen)	-0.168	0.022	8.69×10^{-14}	0.846 (0.809–0.884)	1.12×10^{-10}
TMEM258	BIN	Metabolic disorders (FinnGen)	-0.083	0.020	4.11×10^{-5}	0.920 (0.885–0.958)	4.51×10^{-3}
TMEM258	CD4ET	Metabolic disorders (FinnGen)	-0.070	0.017	4.11×10^{-5}	0.933 (0.902–0.964)	4.51×10^{-3}
TMEM258	CD4NC	Metabolic disorders (FinnGen)	-0.039	0.009	4.11×10^{-5}	0.962 (0.944–0.980)	4.51×10^{-3}
ABHD16A	MONONC	HTN	0.013	0.002	7.11×10^{-12}	1.013 (1.010–1.017)	1.76×10^{-9}
ABHD16A	CD4ET	HTN	0.016	0.002	2.79×10^{-12}	1.016 (1.012–1.021)	7.33×10^{-10}
HSPA1L	CD8S100B	HTN	-0.009	0.002	5.77×10^{-7}	0.991 (0.988–0.995)	3.17×10^{-5}
LY6G5B	NK	HTN	-0.014	0.003	3.17×10^{-7}	0.986 (0.980–0.991)	2.00×10^{-5}

0.8 0.9 1.0 1.1

Odds ratio (log scale)

All displayed associations are one-instrument Wald-ratio estimates (nSNP = 1). Points and horizontal bars denote effect estimates and 95% confidence intervals.

Figure 2. Mendelian randomization prioritizes immune-cell-specific gene-trait associations across metabolic phenotypes. (A) Venn diagram showing the overlap of FDR-significant gene-cell exposures across five metabolic-syndrome component traits: TG, HDL-C, FG, WC, and HTN. Each entry represents a gene-cell exposure rather than a unique gene. Intersections indicate that the same immune-cell-specific gene-expression exposure was associated with more than one component trait by the primary MR analysis. These overlaps were considered evidence of cross-trait recurrence and not proof of biological pleiotropy or shared causality; (B) Flow diagram summarizing the selection of gene-cell exposures for regional mapping. The starting set comprised 3,319 unique eQTL-associated genes represented by 9,117 cell-type-specific instrument records. After matching instruments to the outcome GWAS datasets, 3,195 instrument records were available for the CTG metabolic-syndrome common-factor outcome, 8,437 for the FinnGen metabolic-disorders outcome, and 8,809 for the five component-trait datasets. Primary MR identified 364 FDR-significant gene-cell exposures for the CTG outcome and 134 for the FinnGen outcome. For the component-trait analysis, 54 gene-cell exposures associated with at least three of the five component traits were carried forward, corresponding to 163 gene-cell-trait regions. The ≥ 3-of-5 threshold was used as an exploratory filtering rule to retain recurrent component-trait signals while limiting the number of regions entering downstream mapping; it was not intended to establish biological pleiotropy and was not applied to the CTG or FinnGen branches. As sensitivity counts, 378 exposures met the ≥ 2-of-5 criterion and one exposure met the ≥ 4-of-5 criterion. The final numbers of 203, 123, and 53 represent broad exploratory mapped gene-cell exposures for the CTG, FinnGen, and component-trait groups, respectively. This broad set incorporated both formal Bayesian colocalization findings and associations supported only by the exploratory linkage-disequilibrium screen; it therefore should not be interpreted as a set of formally colocalized associations; (C) Venn diagram showing the overlap of the broad exploratory mapped gene-cell

exposures among the CTG metabolic-syndrome common-factor outcome, the FinnGen metabolic-disorders outcome, and the five component traits. The three sets contained 203, 123, and 53 gene-cell exposures, respectively, with 337 unique gene-cell exposures in their union. Thirty-one gene-cell exposures occurred in at least two mapping groups, including 11 represented in all three groups. After collapsing immune-cell contexts and duplicate outcome records, the 337 gene-cell exposures corresponded to 192 unique genes. Of these, 28 genes were represented in at least two mapping groups and six were represented in all three groups. Accordingly, the 192-gene set was treated as a broad exploratory candidate pool, rather than a set of 192 formally colocalized or causally established genes; (D) Forest plots showing selected primary MR estimates for representative immune-cell-specific gene-trait associations involving *FADS1*, *TMEM258*, *ABHD16A*, *HSPA1L*, and *LY6G5B*. Because every displayed association was based on one genetic instrument, estimates were obtained using the Wald-ratio method. Effect estimates and 95% confidence intervals are reported as β coefficients for quantitative outcomes - the CTG metabolic-syndrome common factor, fasting glucose, and high-density lipoprotein cholesterol - and as odds ratios for binary outcomes - the FinnGen metabolic-disorders endpoint and hypertension. Nominal *P* values and Benjamini-Hochberg FDR-adjusted *P* values are shown. The selected associations illustrate variation in the direction and magnitude of MR estimates across genes, immune-cell contexts, and metabolic outcomes and do not, by themselves, establish causal effects. Complete primary MR results are provided in Supplementary Table 3. Formal approximate Bayes factor and SuSiE colocalization results are provided in Supplementary Table 5A-C, whereas the exploratory linkage-disequilibrium mapping results and classification of the broad candidate set are provided separately in Supplementary Table 5D. CI: Confidence interval; CTG: Complex Trait Genetics; eQTL: expression quantitative trait locus; FDR: false discovery rate; FG: fasting glucose; GWAS: genome-wide association study; HDL-C: high-density lipoprotein cholesterol; HTN: hypertension; LD: linkage disequilibrium; MetS: metabolic syndrome; MR: Mendelian randomization; OR: odds ratio; SuSiE: sum of single effects; TG: triglycerides; WC: waist circumference.

populations according to the similarity of their observed gene-trait association patterns. These descriptive patterns may be influenced by differences in effective eQTL sample size and by instruments shared across cell populations. Because we did not formally test between-cell-type effect heterogeneity, the plots do not establish cell-type-specific regulation or distinct causal mechanisms.

Exploratory functional enrichment and protein-protein interaction network analysis of the broad gene pool

To characterize the biological annotations represented by the broad exploratory gene pool, we performed functional enrichment and PPI network analyses [Figure 4 and Supplementary Table 11]. This pool comprised 192 genes represented by both formally colocalized associations and additional associations retained through the exploratory LD-based screen. GO enrichment analysis identified annotations related to lipid metabolism and nutrient responses, including glycerolipid metabolic processes, responses to nutrients, and phosphatidylcholine biosynthesis. Enriched cellular-component terms included the endoplasmic reticulum membrane, very-low-density lipoprotein particles, and triglyceride-rich plasma lipoprotein particles, whereas molecular-function terms included ubiquitin-like protein ligase binding, nuclear-import signal receptor activity, and nucleocytoplasmic carrier activity [Figure 4A and Supplementary Table 11B]. These enrichment analyses were performed using the broad exploratory 192-gene pool and were not repeated using only the 68 genes represented in the formally colocalized set. Accordingly, the identified terms should be interpreted as descriptive and hypothesis-generating annotations of the selected pool.

KEGG enrichment analysis further identified several lipid-metabolic pathways, including fatty acid metabolism, glycerolipid metabolism, biosynthesis of unsaturated fatty acids, fatty acid elongation, cholesterol metabolism, and lipid and atherosclerosis. Additional enriched annotations involved apoptosis, lysosomal function, ribosomal processes, phosphatidylinositol signaling, ferroptosis, the advanced glycation end-product-receptor for advanced glycation end-product pathway in diabetic complications, natural-killer-cell-mediated cytotoxicity, and antigen processing and presentation [Figure 4B, Supplementary Table 11C]. These findings indicate that the exploratory gene pool encompasses lipid-metabolic, cellular-stress, and immune-related annotations. However, pathway enrichment alone does not establish a shared causal mechanism, biological interaction, or disease-specific pathway activity.

We next constructed a STRING PPI network and applied the MCODE algorithm to identify densely connected network modules [Figure 4C, Supplementary Table 11D and E]. Cluster 1 (red) was dominated by human leukocyte antigen genes involved in antigen processing and presentation. Cluster 2 (blue) contained

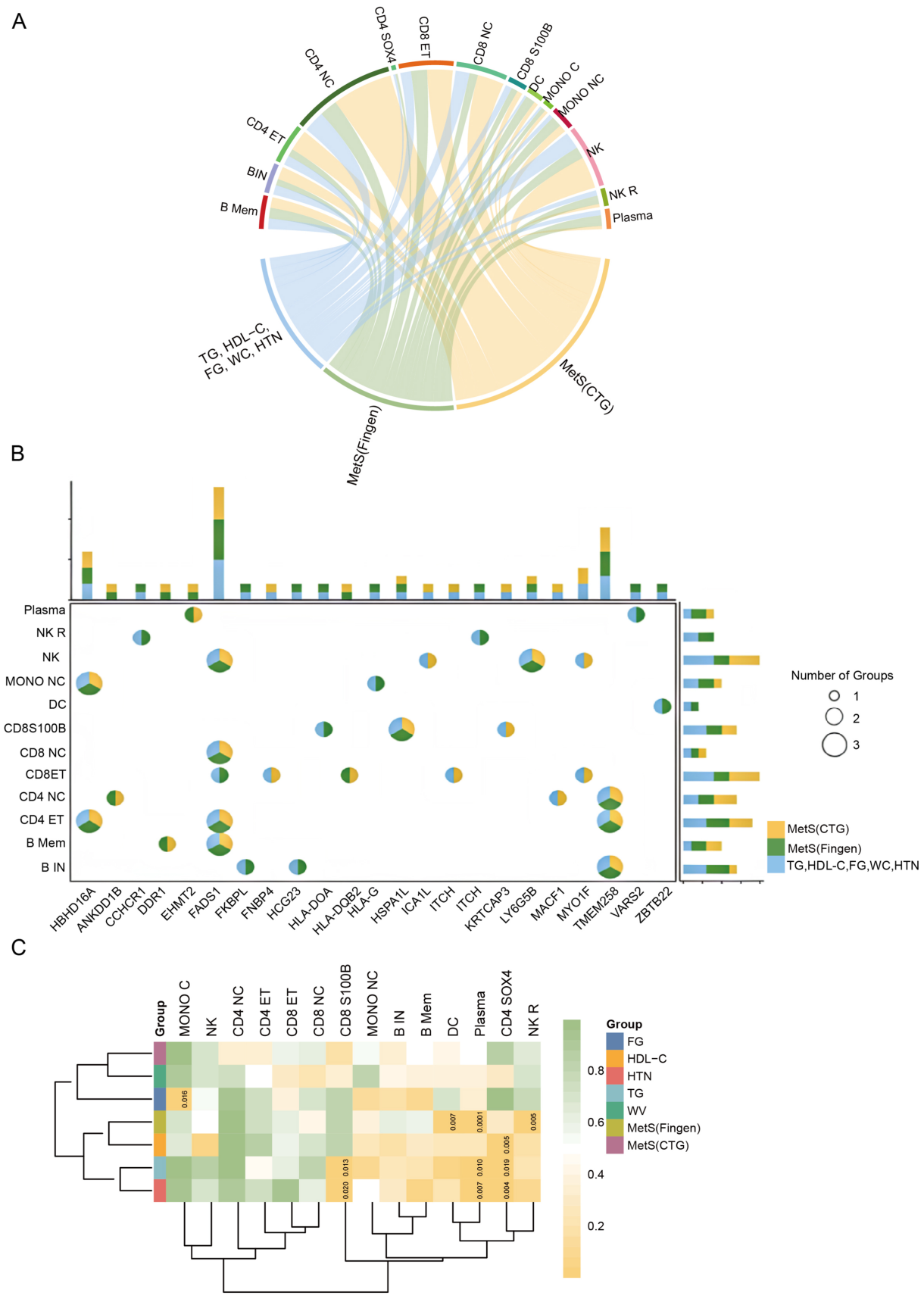


Figure 3. Cross-phenotype and immune cell-resolved patterns of MR-prioritized gene-cell exposures. (A) Circos plot illustrating the relationships between immune-cell populations and metabolic phenotype groups. Links connect immune-cell-specific gene-cell exposures to three phenotype categories: MetS derived from the CTG consortium, MetS derived from FinnGen, and combined cardiometabolic component traits, including TG, HDL-C, FG, WC, and HTN. The plot summarizes the observed overlap of gene-cell exposures across immune-cell contexts and metabolic phenotype groups and does not establish shared biological causality; (B) Bubble plot showing the

number of phenotype groups in which each MR-prioritized gene-cell exposure was detected, stratified by immune-cell population. Bubble size represents the number of phenotype groups (one to three), and color indicates the corresponding phenotype category. The bar plots at the top and right summarize the observed distribution of gene-cell exposures across phenotype groups and immune-cell populations. These summaries are descriptive and should not be interpreted as evidence that any immune-cell population functions as a causal hub; (C) Heatmap displaying the observed distribution of immune-cell-specific gene-cell exposures across metabolic phenotype groups. Rows correspond to metabolic phenotype groups, and columns represent immune-cell populations. Hierarchical clustering reflects similarity in the observed gene-phenotype association patterns. The clustering therefore summarizes detection patterns rather than formally established cell-type-specific regulatory mechanisms. Between-cell-type effect heterogeneity was not formally tested. Differences in the number and distribution of detected associations may reflect unequal effective eQTL sample sizes, statistical power, and genetic instruments shared across cell types. Accordingly, these plots should be interpreted as detection-limited, descriptive cell-resolved patterns and do not establish cell-type-specific causal mediation, lineage specificity, or distinct regulatory compartmentalization. CTG: Complex Trait Genetics; eQTL: Expression quantitative trait locus; FG: fasting glucose; HDL-C: high-density lipoprotein cholesterol; HTN: hypertension; MR: Mendelian randomization; TG: triglycerides; WC: waist circumference.

multiple histone- and chromatin-associated proteins, consistent with a chromatin-regulatory module. Cluster 3 (green) was enriched in ribosomal proteins and was therefore interpreted as a predominantly translation-related module. Cluster 4 (purple) was a smaller and functionally heterogeneous module comprising *DXO*, *EGFL8*, *FKBPL*, and *PRRT1*; therefore, no single biological function was assigned to this cluster. Collectively, the network analysis showed that some MR-prioritized genes were located within interconnected immune-, chromatin-, and translation-related network regions. These topology-based modules should be regarded as hypothesis-generating network structures rather than experimentally validated protein complexes, causal pathways, or therapeutic targets.

Bayesian colocalization and SMR/HEIDI distinguish formally supported associations from exploratory signals

We evaluated 661 MR-prioritized gene-cell-trait regions by regional colocalization. Of these, 139 met the prespecified approximate Bayes factor criterion (PP.H4 ≥ 0.70). SuSiE was additionally applied to 322 regions selected on the basis of PP.H3 ≥ 0.50, and 20 additional associations met the signal-level PP.H4 ≥ 0.70 criterion. Thus, 159 associations involving 68 unique genes constituted the formally colocalized set [Supplementary Table 5A-C].

The previously reported broader set of 439 associations involving 192 genes comprised these 159 formally supported associations and 280 additional exploratory LD-screened associations. The latter did not meet the definition of formal colocalization. We therefore report the 439 associations and 192 genes only as a historical exploratory candidate pool and base claims of colocalization on the 159-association set. Gene-prioritization results derived from the broader pool are presented as exploratory and interpreted in light of this distinction [Supplementary Tables 5D and 9].

SMR results were available for 392 of the 439 associations in the broad exploratory pool, whereas 47 associations lacked an evaluable SMR record and were classified as not evaluated rather than as negative findings. Among the 392 SMR records, 329 remained significant after FDR correction. HEIDI *P* values were evaluable for 388 records; 170 associations were both SMR-FDR significant and had HEIDI $P > 0.05$. The four records without an evaluable HEIDI *P* value were retained as SMR records but excluded from the HEIDI-evaluable denominator [Supplementary Table 6A and B].

Consistent with these aggregate results, the volcano plot illustrated both positive and negative SMR estimates among the evaluable immune-cell-specific gene-trait associations [Figure 5A, Supplementary Table 6A and B]. Forest plots further summarized the FDR-significant SMR associations across fasting glucose, high-density lipoprotein cholesterol, triglycerides, waist circumference, MetS, and hypertension [Figure 5B]. *TMEM258* and *FADS1* showed recurrent SMR associations across multiple immune-cell and metabolic-trait contexts, whereas *LY6G5B* and *ABHD16A* exhibited more restricted or context-dependent patterns. Because

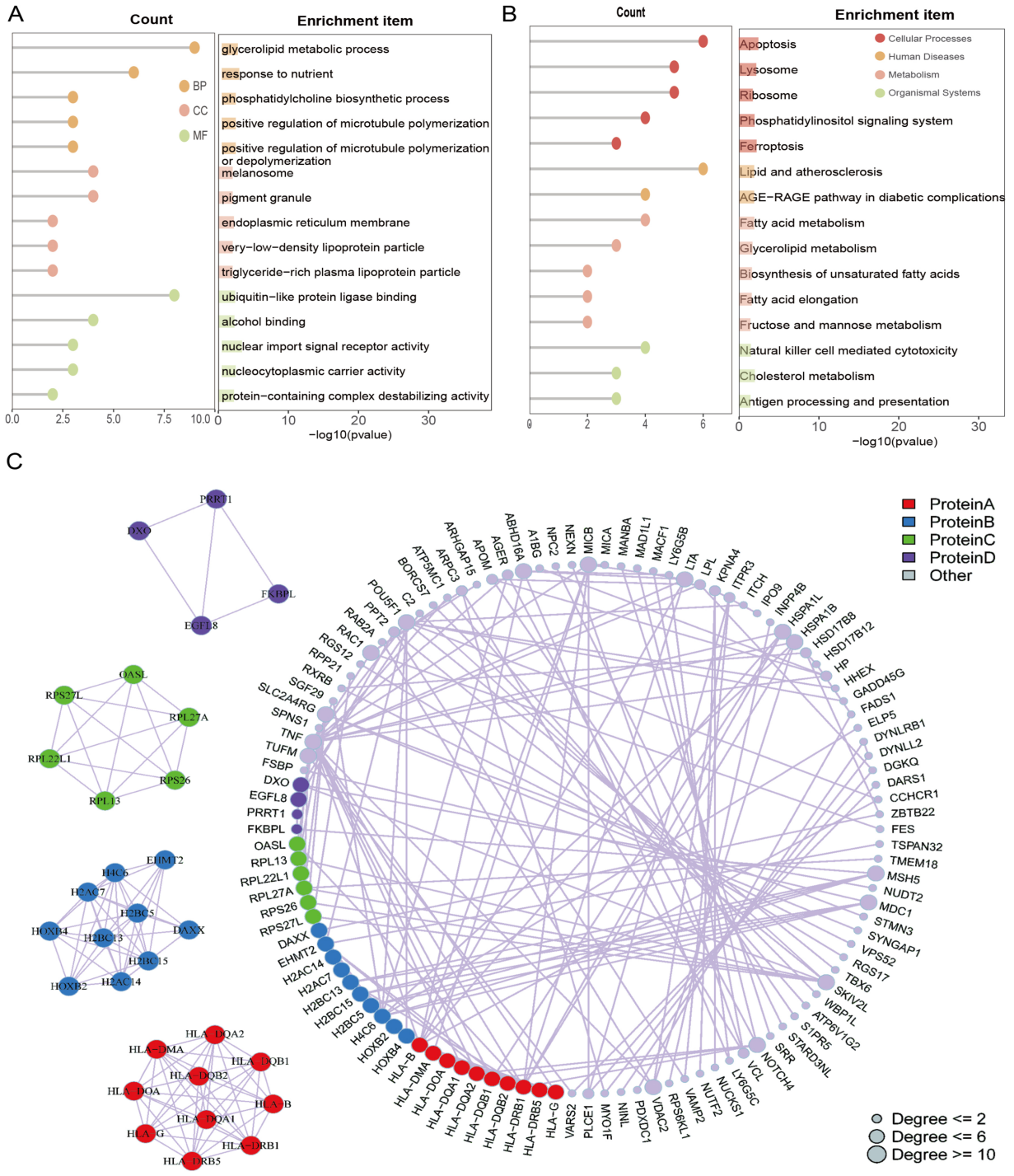


Figure 4. Exploratory enrichment and protein-interaction analysis of the broad candidate pool. All enrichment and network analyses in this figure were performed using the broad exploratory pool of 192 genes. This pool included genes represented by 159 formally colocalized associations involving 68 genes, together with additional associations retained through the exploratory LD-based screen without formal colocalization support. Therefore, the enrichment and PPI results are hypothesis-generating and should not be interpreted as evidence that all 192 genes are formally colocalized or causally implicated. (A) GO enrichment analysis of genes in the broad exploratory pool. The top enriched terms are shown for BP (orange), CC (green), and MF (light green); (B) KEGG pathway enrichment analysis showing the top enriched pathways, including metabolic and immune-related processes. These pathways represent exploratory functional enrichment and may change when the analysis is restricted to the formally colocalized 68-gene set; (C) PPI network of genes in the broad exploratory pool. The right panel shows the global network, with node size indicating interaction degree. The left panels show four MCODE clusters identified from the network: Cluster 1 (red), HLA-complex-related proteins; Cluster 2 (blue), histone- and chromatin-associated proteins; Cluster 3 (green), ribosomal proteins; and Cluster 4 (purple), comprising *DXO*, *EGFL8*, *FKBPL*, and *PRRT1* without a single unified functional annotation. Node colors indicate cluster membership, and node sizes represent the degree of protein interactions. The cluster assignments are descriptive and should not be interpreted as evidence of independent biological modules or causal pathways. BP: Biological process; CC: cellular component; GO: Gene Ontology; HLA: human leukocyte antigen; KEGG: Kyoto Encyclopedia of Genes and Genomes; LD: linkage disequilibrium; MCODE: Molecular Complex Detection; MF: molecular function; PPI: protein-protein interaction.

HEIDI support varied across gene-cell-trait combinations, these results were interpreted as context-dependent statistical support rather than uniformly validated causal effects.

A Sankey diagram was used to summarize the many-to-many relationships among genes, immune-cell contexts, and metabolic phenotypes represented by the FDR-significant SMR associations [Figure 5C]. Fasting glucose, triglycerides, waist circumference, and MetS showed relatively high connectivity within the evaluated association set. This visualization was considered descriptive and was not itself interpreted as evidence of biological pleiotropy or a shared causal mechanism.

GTEx-based tissue-level SMR/HEIDI analyses further showed that some overlapping gene-trait associations were detectable in more than one tissue, although the strength of SMR and HEIDI support was not uniform across tissues [Supplementary Table 8]. These findings provided evidence of cross-tissue support for selected associations rather than universal cross-tissue robustness and did not localize the causal effect to the immune compartment.

For cross-platform validation, two-sample MR analyses were additionally performed using blood eQTL data from the eQTLGen consortium [Figure 5D]. For *FADS1*, the blood-eQTL analysis associated genetically proxied higher expression with higher triglycerides and lower HDL-C in selected comparisons, whereas the magnitude and support varied by outcome and immune-cell context [Supplementary Table 7]. *LY6G5B* and *ABHD16A* also showed concordant estimates for selected outcomes. These analyses provided supportive cross-platform replication but did not replace formal colocalization or HEIDI assessment.

Multi-layer prioritization highlights *FADS1* within the exploratory candidate pool

The broader set of 192 candidate genes was subsequently subjected to exploratory multi-layer prioritization [Figure 6A, Supplementary Table 9A and B]. The composite score comprised five prespecified components: recurrence of primary MR support across the mapping groups, pathway-enrichment evidence, membership in prioritized MCODE modules, PPI network connectivity, and evidence based on known compound-target annotations. Formal colocalization and SMR/HEIDI results were displayed as independent validation evidence and were not included in the composite score. Because the input pool included LD-screened associations without formal colocalization support, the resulting scores and Tier assignments are exploratory rankings rather than validated causal-gene classifications.

Application of the corrected, data-consistent thresholds classified 10 genes as Tier 1 (total score ≥ 1.00), 126 as Tier 2 (0.35- < 1.00), and 56 as Tier 3 (< 0.35). *HSPA1L* received the highest composite score (2.45), followed by *FADS1* (2.15), *DDR1* (1.80), *TMEM258* (1.75), and *ABHD16A* (1.55) [Figure 6B]. *FADS1* received component scores of 0.75 for MR recurrence, 0.30 for pathway evidence, 0 for MCODE module membership, 0.10 for PPI connectivity, and 1.00 for druggability evidence [Figure 6B]. Thus, *FADS1* was classified as a Tier 1 candidate but was not the highest-ranked gene.

To evaluate expression patterns in a clinical context, transcriptomic data from PBMCs in the GSE200744 cohort were analyzed. *FADS1* expression was significantly higher in individuals with MetS compared with pre-metabolic syndrome (preMetS) subjects, whereas no significant difference was observed between normal and preMetS groups [Figure 6C]. In contrast, expression levels of *HSPA1L* and *TMEM258* did not differ significantly across normal, preMetS, and MetS groups [Figure 6D and E]. Cell-type-specific analysis further demonstrated that *FADS1* expression was significantly increased in $CD14^+$ monocytes from obese individuals compared with lean controls in the GSE32575 dataset [Figure 6F], indicating cell-type-specific regulation associated with metabolic status.

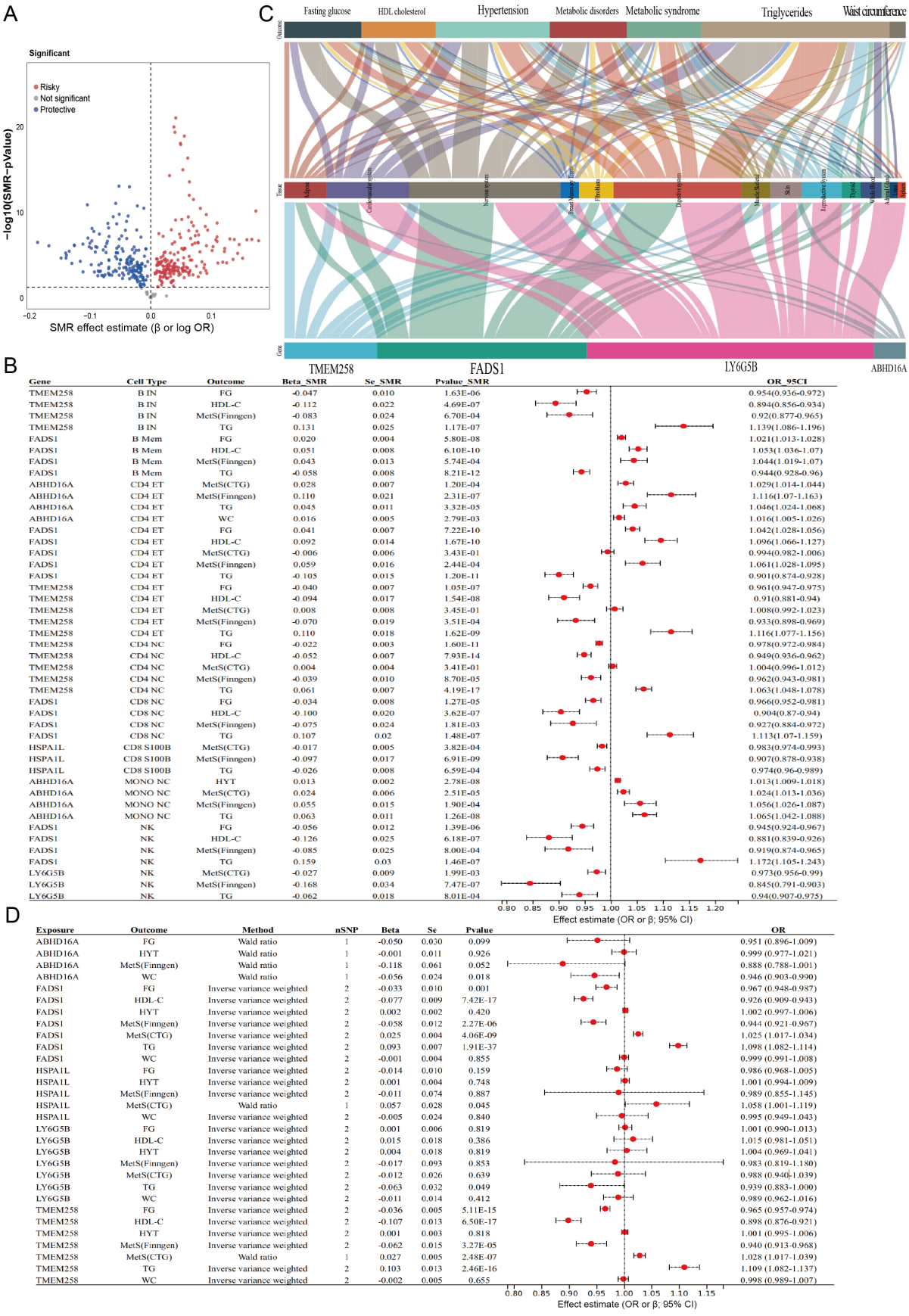


Figure 5. Cross-platform SMR and MR analyses of prioritized gene-trait associations. (A) Volcano plot showing SMR results integrating immune-cell-specific eQTLs with GWAS summary statistics for metabolic traits. The x-axis represents the SMR effect estimate, expressed as β for continuous outcomes or log odds ratios for binary outcomes, and the y-axis shows -log10(SMR *P* values). Each point corresponds to a gene-trait association evaluated across immune-cell contexts. Red and blue dots indicate positive and negative associations, respectively, after FDR correction, whereas grey dots denote associations that did not meet the FDR threshold; (B) Forest plots

summarizing FDR-significant immune-cell-specific SMR associations across FG, HDL-C, TG, WC, MetS, and HTN. Effect estimates and 95% confidence intervals are shown for the associations displayed in the panel. β coefficients are reported for continuous outcomes, whereas odds ratios are reported for binary outcomes. *TMEM258* and *FADS1* showed recurring associations across multiple lipid-related traits and metabolic-syndrome-related outcomes, whereas *LY6G5B* and *ABHD16A* showed more restricted or context-dependent patterns; (C) Sankey diagram illustrating the many-to-many relationships among genes, immune-cell contexts, and metabolic phenotypes represented by FDR-significant SMR associations. The diagram is descriptive and summarizes the observed structure of the evaluated association set; it does not establish shared immune-mediated regulation, biological pleiotropy, or a common causal mechanism. GTEx-based tissue-level SMR/HEIDI analyses provided additional cross-tissue evidence for selected gene-trait associations, although the strength of support varied across tissues [Supplementary Table 8]; (D) Forest plots showing two-sample MR estimates obtained using blood eQTLs from the eQTLGen consortium as exposure instruments. Effect estimates are presented as odds ratios for binary outcomes or β coefficients for continuous outcomes, with 95% confidence intervals. The panel displays selected gene-trait pairs involving *TMEM258*, *FADS1*, *LY6G5B*, and *ABHD16A* for visualization. Directionally concordant estimates provide cross-platform consistency with the immune-cell-specific SMR findings but do not constitute independent causal validation or replace formal colocalization and HEIDI assessment. Complete eQTL Gene validation results are provided in Supplementary Table 7. CI: Confidence interval; eQTL: expression quantitative trait locus; FDR: false discovery rate; FG: fasting glucose; GWAS: genome-wide association study; HDL-C: high-density lipoprotein cholesterol; HEIDI: heterogeneity in dependent instruments; HTN: hypertension; MetS: metabolic syndrome; MR: Mendelian randomization; OR: odds ratio; SMR: summary-data-based Mendelian randomization; TG: triglycerides; WC: waist circumference.

Following the genetic and molecular prioritization of *FADS1*, exploratory molecular docking was performed to assess the predicted structural compatibility of selected approved or investigational compounds with the FADS1 structural model. To explore potential structural compatibility with existing compounds, 5,903 approved or investigational small molecules were screened against the FADS1 structural model using AutoDock Vina. Five compounds - Xaliproden, ONO-RS-411, Lumacaftor, Eltrombopag, and Rolapitant - were selected for pose visualization [Figure 6G, Supplementary Table 9C and D].

FADS1 exhibits cross-tissue dysregulation and associates with metabolic and inflammatory phenotypes

To further characterize the biological relevance of *FADS1*, we systematically examined its expression patterns across multiple tissues and metabolic disease contexts [Figure 7]. Analysis of bulk transcriptomic data from the GTEx database revealed that *FADS1* is broadly expressed across human tissues, with relatively higher expression in metabolically active tissues, including adipose tissue and liver [Figure 7A]. Consistent with its potential immunometabolic role, cell-type-resolved data from the Human Protein Atlas demonstrated that *FADS1* expression is enriched in immune cell subsets, particularly within monocyte and myeloid lineages [Figure 7B].

We next assessed *FADS1* expression in independent transcriptomic datasets representing different metabolic conditions. No significant differences were observed in skeletal muscle [Figure 7C]. In GSE159924, hepatic *FADS1* expression did not differ significantly between obese participants without NAFLD (Ob-NL) and lean participants without NAFLD (Lean-NL), whereas expression was significantly lower in obese participants with NAFLD (Ob-NAFLD) than in the Lean-NL group ($P < 0.05$; Figure 7D). In GSE126848, hepatic *FADS1* expression was significantly lower in the obese, NAFLD, and NASH groups than in normal controls [Figure 7E]. These findings indicate that hepatic expression differences varied across cohorts and clinical subgroups. In GSE141432, *FADS1* expression was significantly lower in visceral adipose tissue from obese participants and participants with T2D than in lean controls [Figure 7F]. In GSE24883, *FADS1* expression was significantly lower in the obese and MetS groups than in the lean group in visceral adipose tissue, whereas no significant differences were indicated in subcutaneous adipose tissue [Figure 7G].

To evaluate clinical relevance, we further analyzed data from the metabolically healthy *vs.* unhealthy obesity (MHUO) cohort. *FADS1* expression was significantly decreased in metabolically unhealthy obese (MUO) individuals compared with metabolically healthy obese (MHO) subjects [Figure 7H], suggesting a link between *FADS1* expression and metabolic health status. Correlation analyses demonstrated that *FADS1* expression was significantly associated with key metabolic and inflammatory traits, including triglycerides

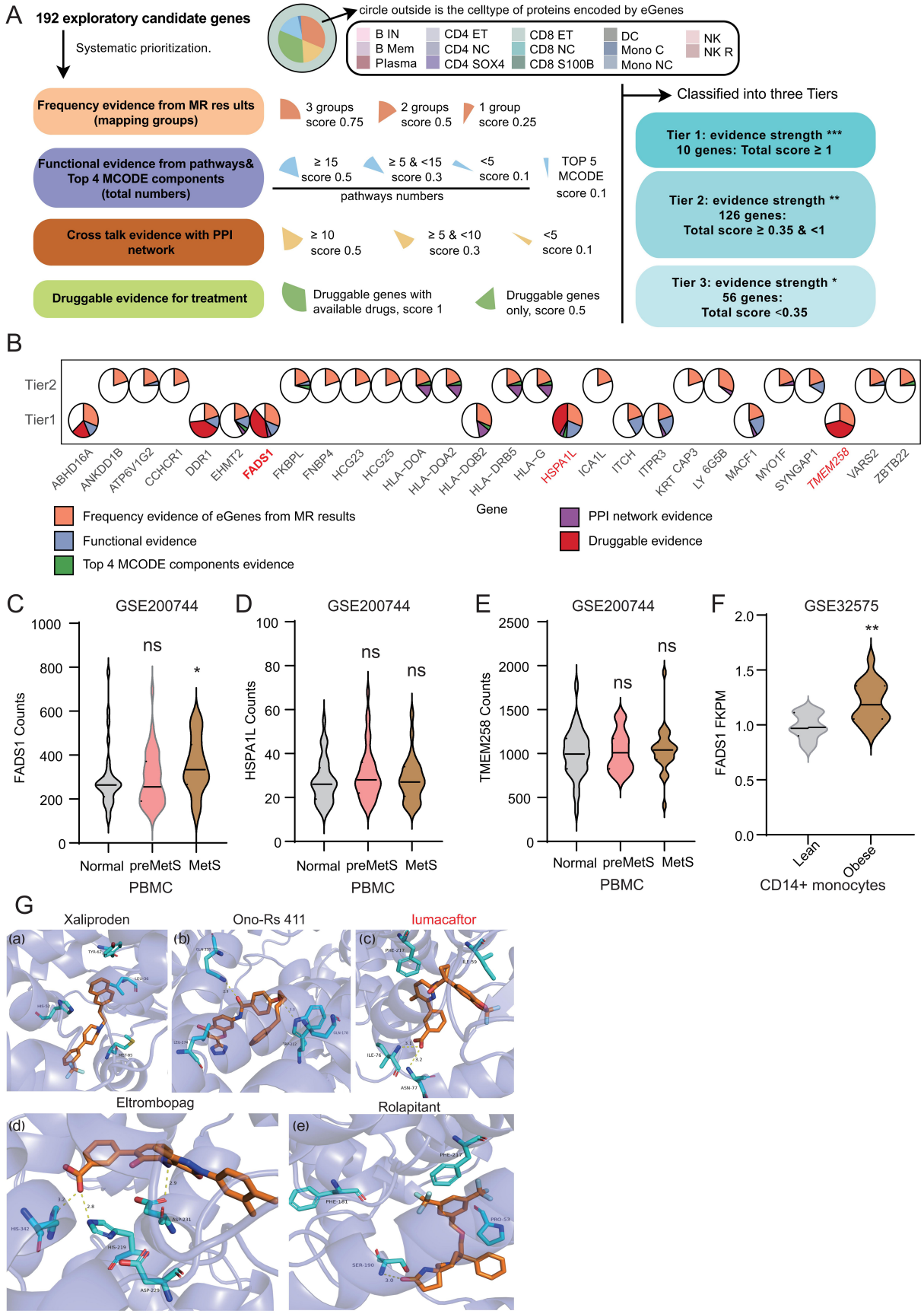


Figure 6. Exploratory prioritization of candidate genes and structure-based screening of compounds against *FADS1*. (A) Scoring framework applied to a broad exploratory pool of 192 unique genes derived from 439 gene-cell-trait association records. This pool included 159 associations meeting the formal Bayesian colocalization criterion and 280 additional associations retained through an exploratory LD-based screen. These numbers refer to association records, whereas 192 refers to unique genes. The resulting score was used to rank candidates for follow-up and does not represent the probability that a gene is causal or establish formal colocalization for every

association contributing to the candidate pool; (B) Contributions of the prespecified MR-recurrence, pathway-enrichment, MCODE-module, PPI, and druggability components to the exploratory composite scores. *HSPA1L* ranked first (2.45), followed by *FADS1* (2.15). Formal colocalization and SMR/HEIDI findings were evaluated separately and were not included as independent components of the composite score; (C-F) Expression patterns of selected prioritized genes in independent transcriptomic datasets. These observational expression results provide biological context but do not establish immune-cell mediation, effector-gene status, or a lipid-remodeling mechanism. *FADS1* was highlighted because it showed additional transcriptomic and lipid-related support, despite *HSPA1L* having the highest composite score. Statistical significance in panels C-F is indicated as follows: $^{*}P < 0.05$, $^{**}P < 0.01$, and $^{***}P < 0.001$; ns, not statistically significant ($P \geq 0.05$). For panel C, the indicated comparisons are preMetS *vs.* Normal and MetS *vs.* preMetS. For panels D-E, comparisons were made against the Normal group; for panel F, the Obese group was compared with the Lean group; (G) Exploratory structure-based virtual docking of five displayed compounds with an AlphaFold-predicted FADS1 protein structure. Xaliproden (a), Ono-RS-411 (b), lumacaftor (c), eltrombopag (d), and rolapitant (e) were selected from a 5,903-compound screening library based on predicted binding scores generated with AutoDock Vina. The compounds are shown for illustrative visualization and should not be interpreted as uniformly FDA-approved FADS1 ligands. The docking pocket was computationally defined using the grid centered at x = 1, y = -8, and z = 0, with dimensions of 35 Å × 30 Å × 34 Å. Ligands are shown in orange and FADS1 residues in cyan; hydrogen bonds and hydrophobic interactions are annotated. The docking screen was hypothesis-generating, and the complete ranked output was not available in the displayed panel. No biochemical binding assay, target-engagement experiment, substrate redocking validation, or functional activity assay was performed. The docking scores therefore indicate structural compatibility only and do not establish binding, target engagement, pharmacological activity, or therapeutic tractability. LD: Linkage disequilibrium; MCODE: Molecular Complex Detection; MetS: metabolic syndrome; MR: Mendelian randomization; ns: not statistically significant; preMetS: pre-metabolic syndrome; PPI: protein-protein interaction; T2D: type 2 diabetes.

and C-reactive protein (CRP) [Figure 7I and J]. Notably, *FADS1* expression was also significantly associated with macrophage abundance in omental adipose tissue [Figure 7K], supporting its involvement in immune-metabolic interactions.

To provide an integrated view, we examined the global associations between *FADS1* expression and clinical phenotypes. Heatmap analysis revealed correlations between *FADS1* and multiple biological domains, including adipose dysfunction, inflammation, lipid metabolism, and insulin sensitivity [Figure 7L]. Summary analysis of correlation coefficients further confirmed that *FADS1* is linked to key metabolic parameters, particularly inflammatory markers and lipid-related traits [Figure 7M]. Across independent datasets, *FADS1* expression varied by tissue and was associated with metabolic status or clinical measures in selected within-cohort analyses [Figure 7]. GTEx tissue distribution and disease-associated expression comparisons address different questions. Because the cohorts differed in participants, assay platforms, and analytical processing, we did not formally compare disease effects between tissues. These observations provide context for *FADS1* prioritization but do not establish coordinated cross-tissue regulation, immune-cell mediation, or a tissue-specific causal mechanism.

Nutrigenetic and cross-sectional NHANES analyses provide context for the serum AA/DGLA proxy

To provide additional context for the relationship between dietary PUFA exposure and systemic fatty acid composition, we integrated published nutrigenetic evidence with population-level analyses using NHANES 2013-2014 data [Figure 8 and Supplementary Tables 12-14]. The conceptual framework in Figure 8A illustrates proposed relationships among dietary PUFA exposure, variation in the fatty acid desaturase (FADS) locus, and PUFA metabolism; these mechanistic relationships were not directly tested in the present study. Published human studies have reported context-dependent interactions between *FADS1*-region variants, dietary PUFA composition, lipid traits, adiposity, inflammatory phenotypes, and metabolic risk [Figure 8B]. Hellstrand *et al.* reported interactions between dietary PUFA intake and FADS rs174547 in relation to blood lipid concentrations[16]. Dumont *et al.* found that dietary LA intake modified associations of rs174547 with HDL-cholesterol, waist circumference, and body mass index (BMI)[17]. Park *et al.* reported interactions between dietary fat intake and FADS variants in relation to MetS in two Korean cohorts[18]. In the FADSDIET2 trial, Lankinen *et al.* observed genotype-dependent responses to LA- and ALA-enriched diets[19]. Meuronen *et al.* characterized plasma phospholipid changes during a high-LA intervention, although the genotype-diet interactions did not remain significant after multiple-testing correction[20]. Vaittinen *et al.* reported genotype-dependent effects of an LA-enriched diet on adipose tissue inflammatory gene expression[21]. These reports were considered supporting background evidence rather than direct validation of immune-cell-specific *FADS1* effects.

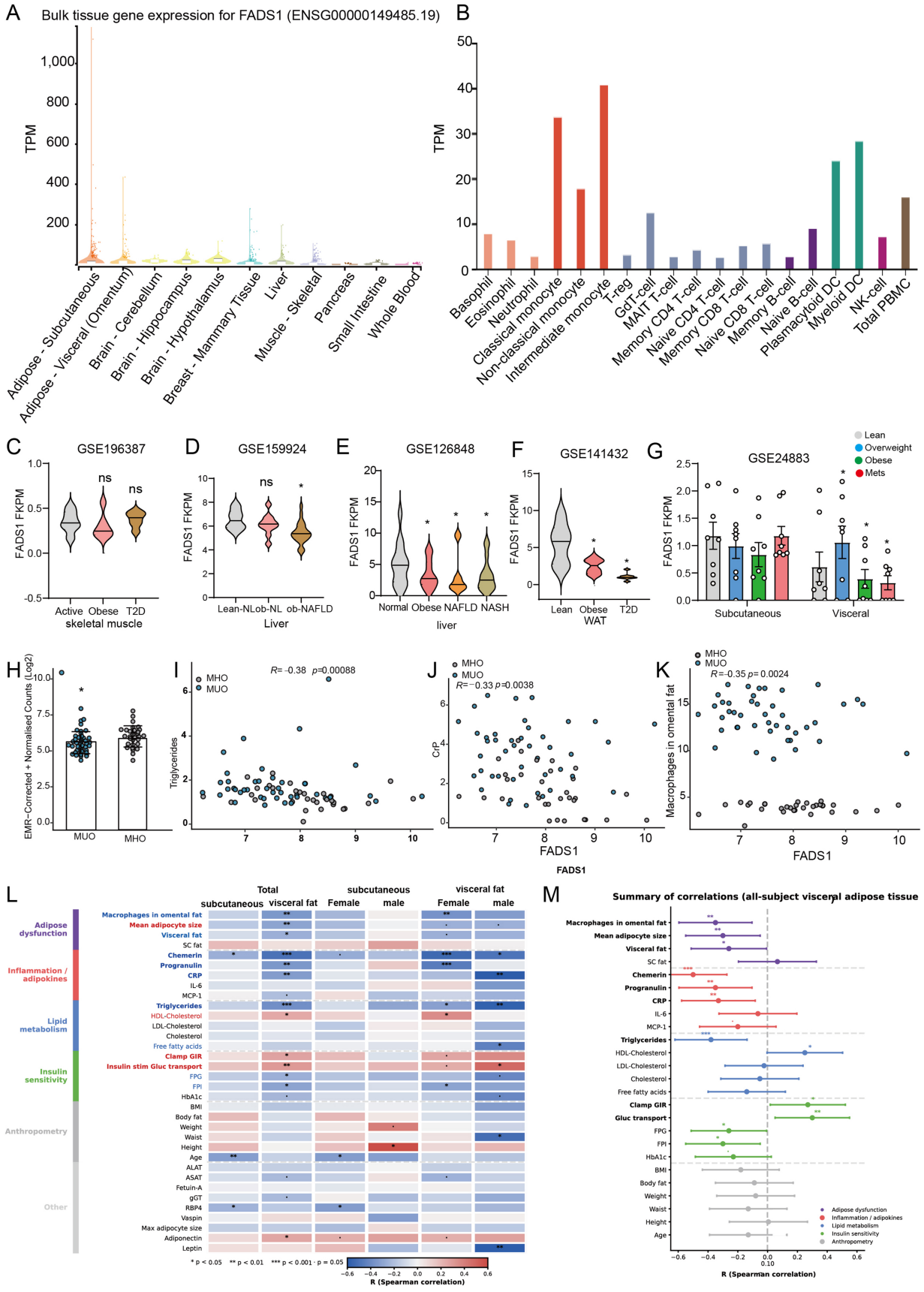


Figure 7. *FADS1* expression and clinical associations across independent datasets. (A) Tissue distribution of *FADS1* expression across GTEx tissues. *FADS1* expression was relatively high in adipose and liver tissues. These data describe baseline tissue distribution and do not indicate the direction of disease-associated expression changes or identify the tissue mediating the genetic associations; (B) *FADS1* expression across peripheral immune-cell populations in the HPA dataset; (C-G) Within-dataset comparisons of *FADS1* expression in metabolic conditions: (C) *FADS1* expression in skeletal muscle from lean physically active participants (Active), participants with obesity (Obese), and participants with obesity and type 2 diabetes (T2D) in GSE196387 (*n* = 6 per group); (D) Hepatic *FADS1* expression in lean

participants without NAFLD (Lean-NL), obese participants without NAFLD (Ob-NL), and obese participants with NAFLD (Ob-NAFLD) in GSE159924; (E) liver across normal, obese, NAFLD, and NASH groups in GSE126848; (F) visceral adipose tissue across lean, obese, and T2D groups in GSE141432; and (G) subcutaneous and visceral adipose tissue in obesity in GSE24883. The reference groups for the annotated comparisons were Active in panel C, Lean-NL in panel D, normal in (E), and Lean in (F). In (G), the Overweight, Obese, and MetS groups were compared separately with the Lean group within each adipose depot. $^{*}P < 0.05$, $^{**}P < 0.01$, and $^{***}P < 0.001$; ns, not statistically significant ($P \geq 0.05$); (H-M) Within-cohort expression comparisons and correlations between *FADS1* expression and metabolic or inflammatory measures in the metabolically healthy *vs.* unhealthy obesity cohort. Panels H-M were analyzed within the indicated cohort and were not combined with the other datasets. In panel L, each cell represents the Spearman correlation between *FADS1* expression and the indicated clinical measure within the tissue and participant subgroup specified by the column heading. Colors indicate the correlation coefficients. Asterisks indicate *P* values for testing the null hypothesis of zero correlation: $^{*}P < 0.05$, $^{**}P < 0.01$, and $^{***}P < 0.001$. Because these datasets differed in tissue source, cohort composition, sample size, experimental platform, and normalization procedure, expression levels and effect directions should not be compared directly across panels. No formal tissue-by-disease interaction model or cross-tissue interaction test was performed. Accordingly, these descriptive expression and correlation analyses do not establish the tissue mediating the genetic associations, immune-cell-specific causality, or a disease-wide immune-*vs.*-metabolic-tissue expression pattern. GTEx: Genotype-Tissue Expression; HPA: Human Protein Atlas; Lean-NL: lean participants without NAFLD; MetS: metabolic syndrome; MHO: metabolically healthy obesity; MHUO: metabolically healthy versus unhealthy obesity; MUO: metabolically unhealthy obesity; NAFLD: non-alcoholic fatty liver disease; NASH: non-alcoholic steatohepatitis; Ob-NL: obese participants without NAFLD; T2D: type 2 diabetes.

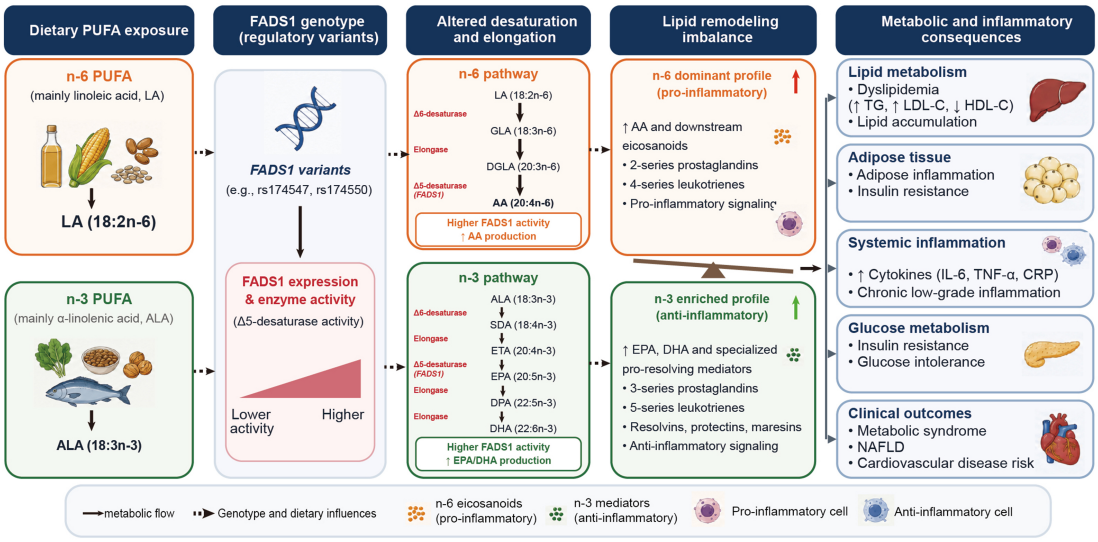
We next evaluated associations between dietary PUFA intake and the serum log-transformed AA-to-DGLA ratio, hereafter referred to as the serum log(AA/DGLA) proxy. This ratio was used as an indirect and non-gene-specific proxy related to Δ5-desaturase activity and systemic PUFA composition, rather than as a direct measurement of FADS1 enzymatic activity. Figure 8C displays the associations for four dietary exposures: LA, ALA, combined EPA + DHA, and the LA/(ALA + EPA + DHA) ratio. Higher combined EPA + DHA intake was nominally associated with a higher serum log(AA/DGLA) proxy (β = 0.0232, nominal $P = 0.045$) [Supplementary Table 12B]. Dietary LA, ALA, and the LA/(ALA + EPA + DHA) ratio were not significantly associated with the proxy. Separate estimates for EPA and DHA are provided in Supplementary Table 13.

We next described the circulating fatty acid components across tertiles of the serum log(AA/DGLA) proxy. Participants in higher proxy tertiles had higher circulating AA and lower DGLA concentrations, as expected from the mathematical construction of the ratio [Figure 8D]. EPA and DHA distributions were also displayed. Because AA and DGLA are components of the ratio used to define the tertiles, these comparisons were treated as descriptive component-level analyses and not as independent validation of Δ5-desaturase activity or *FADS1*-specific function.

We then examined cross-sectional associations between the serum log(AA/DGLA) proxy and cardiometabolic traits using standardized survey-weighted regression models [Figure 8E and F]. Higher proxy values were associated with lower BMI (standardized β = -0.131, FDR = 3.32×10^{-4}) and waist circumference (β = -0.115, FDR = 2.81×10^{-4}). Inverse associations were also observed for triglycerides (β = -0.332, FDR = 2.83×10^{-6}), the TG/HDL-C ratio (β = -0.328, FDR = 4.47×10^{-6}), total cholesterol, low-density lipoprotein cholesterol (LDL-C), and non-high-density lipoprotein cholesterol (non-HDL-C), whereas HDL-C was positively associated with the proxy. No significant associations were observed for glycated hemoglobin (HbA1c) or fasting glucose after multiple-testing correction. The proxy was additionally associated with lower diastolic blood pressure (β = -0.080, FDR = 2.49×10^{-3}); the inverse association with systolic blood pressure was nominal but did not remain significant after correction.

Exploratory inflammatory analyses showed inverse associations between the serum log(AA/DGLA) proxy and white blood cell count (β = -0.101, FDR = 1.08×10^{-2}), neutrophil count (β = -0.095, FDR = 6.63×10^{-3}), and neutrophil-to-lymphocyte ratio (NLR; β = -0.041, FDR = 4.02×10^{-2}). Associations with monocyte count and monocyte-to-lymphocyte ratio were not significant after multiple-testing correction.

A

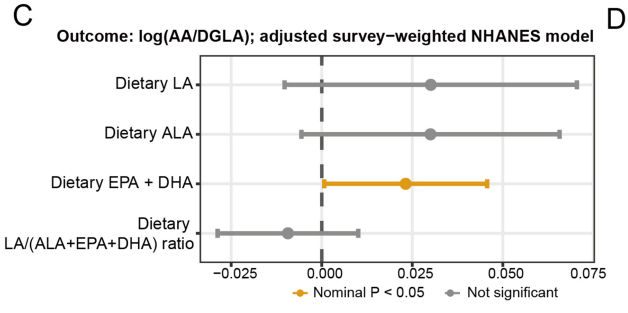


B

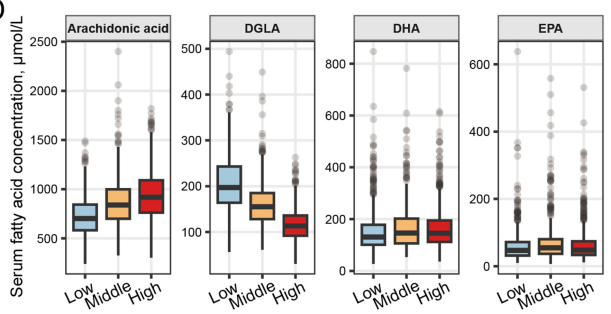
Study (Year)	Study design / Population	Key SNP (Gene)	Dietary factor	Interaction direction (Effect on risk/trait)	Key phenotype(s)	Main interaction message
Hellstrand et al., 2012	Cohort European adults	***FADS rs174547 (FADS1 region)***	**Long-chain n-3 PUFA intake**	**↓ Protective** (improves lipid profile)	LDL, HDL LDL-C / HDL-C	PUFA intake modifies FADS–lipid associations
Dumont et al., 2018	Population / meta-analysis Multiple populations	***FADS1 rs174547***	**Linoleic acid intake**	**↑ Risk-increasing** (adverse lipid / obesity traits)	HDL HDL-C / BMI / waist	LA intake modulates FADS associations with obesity/lipid traits
Park et al., 2019	Cross-sectional cohort Korean adults	***FADS1 rs174547 / FADS haplotype***	**Total fat intake**	**↑ Risk-increasing** (higher MetS risk)	Metabolic syndrome	Dietary fat modifies FADS-related MetS susceptibility
Lankinen et al., 2021	Dietary intervention Finnish adults	***FADS1 rs174550***	**High LA / high ALA diets**	**Genotype-dependent** (metabolic responses vary by genotype)	Metabolic responses	Genotype modifies response to PUFA-rich diets
Meuronen et al., 2022	Dietary intervention Finnish adults	***FADS1 rs174550***	**High-LA diet**	**Genotype-dependent** (remodeling of PUFA composition)	Plasma phospholipid PUFA	Genotype-dependent PUFA remodeling
Vaittinen et al., 2022	Dietary intervention Finnish adults	***FADS1 variant***	**Linoleic acid intake**	**↑ Risk-increasing** (inflammation)	Adipose tissue inflammation	FADS1 genotype may modify LA-induced inflammatory response

↓ Protective interaction ↑ Risk-increasing interaction Genotype-dependent interaction

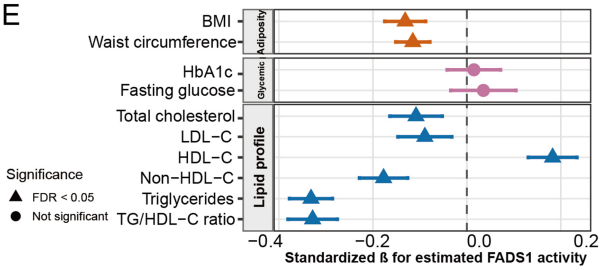
C



D



E



F

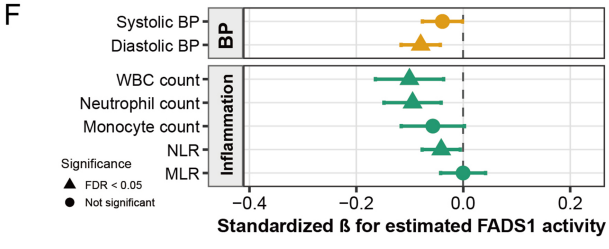


Figure 8. Nutrigenetic evidence and cross-sectional population associations involving the FADS locus and polyunsaturated fatty acid metabolism. (A) Conceptual framework illustrating proposed relationships among dietary PUFA exposure, *FADS1* genetic variation, PUFA desaturation and elongation pathways, and cardiometabolic phenotypes. These mechanistic links were not directly tested in the present study. Conversion of precursor fatty acids into downstream long-chain PUFAs and lipid mediators is shown as a biological hypothesis rather than a demonstrated effect of immune-cell *FADS1* expression; (B) Summary of previously published human nutrigenetic studies

reporting gene-diet interactions involving *FADS1*-region variants and dietary fatty-acid exposure. These studies provide context for possible interactions between genetic variation and dietary PUFA composition, but the reported effects may vary according to population, diet, outcome, and genetic variant; (C) Associations between dietary PUFA intake and the serum log-transformed AA-to-DGLA ratio [serum log(AA/DGLA)] in NHANES 2013-2014. Points and error bars represent standardized regression coefficients and 95% confidence intervals from survey-weighted linear regression models adjusted for age, sex, race and ethnicity, and total energy intake, accounting for the complex sampling design. Four dietary exposures are displayed: LA, ALA, combined EPA + DHA, and the LA/(ALA + EPA + DHA) ratio. Separate EPA and DHA estimates are reported in Supplementary Table 13A. Orange indicates nominal $P < 0.05$, whereas grey indicates nominal $P \geq 0.05$. The LA/(ALA + EPA + DHA) ratio represents selected dietary fatty acids and should not be interpreted as a comprehensive ratio of total dietary n-6 to total dietary n-3 fatty acids; (D) Descriptive distribution of circulating PUFA components across tertiles of the serum log(AA/DGLA) proxy in NHANES participants. Because AA and DGLA are mathematical components of the ratio used to define the tertiles, these comparisons are expected component-level descriptions and should not be interpreted as independent validation of the ratio-based associations. DHA and EPA distributions are also shown; (E) Associations between the serum log(AA/DGLA) proxy and adiposity, glycaemic, and lipid-related traits in NHANES 2013-2014. Higher serum log(AA/DGLA) was associated with lower BMI, waist circumference, total cholesterol, LDL-C, non-HDL-C, triglycerides, and TG/HDL-C ratio, and with higher HDL-C. No significant associations were observed for HbA1c or fasting glucose after multiple-testing correction. Standardized β coefficients and 95% confidence intervals are shown. Triangles indicate FDR-adjusted significance (FDR < 0.05), whereas circles indicate non-significant associations. The serum log(AA/DGLA) measure is an indirect, non-gene-specific proxy that may be influenced by diet, *FADS2*, other enzymes, and metabolic clearance; (F) Associations between the serum log(AA/DGLA) proxy and blood pressure and inflammatory traits in NHANES 2013-2014. Higher serum log(AA/DGLA) was inversely associated with diastolic blood pressure, white blood cell count, neutrophil count, and NLR, whereas monocyte count and monocyte-to-lymphocyte ratio (MLR) were not significantly associated after multiple-testing correction. These observational associations should not be interpreted as evidence that increasing *FADS1* expression is beneficial or that the proxy directly measures FADS1 enzymatic activity. The favorable proxy associations also differ from the modestly lipid-adverse direction observed in some expression-based genetic analyses, supporting a context-dependent interpretation of the FADS gene cluster. (A and B) were prepared with AI assistance using OpenAI Codex and subsequently assembled and edited in Adobe Illustrator. Details are provided in the AI and AI-assisted tools statement. AA: Arachidonic acid; AI: artificial intelligence; ALA: α-linolenic acid; BMI: body mass index; BP: blood pressure; CI: confidence interval; CRP: C-reactive protein; DGLA: dihomo-γ-linolenic acid; DHA: docosahexaenoic acid; DPA: docosapentaenoic acid; EPA: eicosapentaenoic acid; ETA: eicosatetraenoic acid; FADS: fatty acid desaturase; *FADS1*: fatty acid desaturase 1; *FADS2*: fatty acid desaturase 2; FDR: false discovery rate; GLA: γ-linolenic acid; HbA1c: glycated haemoglobin; HDL: high-density lipoprotein; HDL-C: high-density lipoprotein cholesterol; IL-6: interleukin-6; LA: linoleic acid; LDL: low-density lipoprotein; LDL-C: low-density lipoprotein cholesterol; MetS: metabolic syndrome; MLR: monocyte-to-lymphocyte ratio; NAFLD: non-alcoholic fatty liver disease; NHANES: National Health and Nutrition Examination Survey; NLR: neutrophil-to-lymphocyte ratio; non-HDL-C: non-high-density lipoprotein cholesterol; PUFA: polyunsaturated fatty acid; SDA: stearidonic acid; SNP: single-nucleotide polymorphism; TG: triglycerides; TNF-α: tumour necrosis factor-α; WBC: white blood cell. The terms n-3 and n-6 denote the omega-3 and omega-6 fatty acid families, respectively; rs denotes a reference SNP identifier.

These NHANES findings describe population-level associations of an indirect serum fatty acid proxy with adiposity, lipid, blood-pressure, and inflammatory traits. The proxy is not gene-specific and may be influenced by dietary intake, *FADS2*, other enzymes, and metabolic clearance. In addition, its favorable cross-sectional associations differed from the modestly lipid-adverse direction observed in some expression-based genetic analyses. Accordingly, these results support a context-dependent interpretation of the FADS locus and do not establish that increasing *FADS1* expression or activity would be therapeutically beneficial.

DISCUSSION

By integrating immune-cell-resolved cis-eQTLs with metabolic-trait GWAS, we identified gene-cell-trait associations and prioritized loci for further study. Formal Bayesian colocalization supported a subset of these associations, whereas the larger candidate set included signals retained through an exploratory screening criterion. These analyses provide cell-resolved genetic context for metabolic traits but do not establish that the profiled immune cells mediate the observed effects. *FADS1* was nominated as a candidate at a locus linked to PUFA metabolism[21]; its specific contribution and the relevant cellular compartment remain to be determined.

The distribution of detected associations differed across immune-cell populations. These patterns should be interpreted in light of differences in effective eQTL sample size and the sharing of genetic instruments across cell types. We did not formally test between-cell-type effect heterogeneity for shared instruments. Genetic regulatory effects can be shared across tissues as well as exhibit tissue specificity[22]. Therefore, detecting an eQTL in an immune-cell population does not, by itself, establish that this population mediates the

corresponding metabolic association. Accordingly, the present results do not establish lineage-specific causal mechanisms or distinguish immune-cell mediation from shared cross-tissue regulation. The enrichment, protein-interaction network, and composite prioritization analyses were performed on the broad exploratory pool of 192 genes, which included candidates represented only by LD-screened associations. Formal Bayesian colocalization supported 159 gene-cell-trait associations involving 68 genes, whereas the broader pool contained 439 association records. Accordingly, the enriched pathways, network modules, and priority scores should be viewed as tools for generating follow-up hypotheses, not as evidence of causal immune-cell programs. These results could change substantially if the analyses were restricted to the 68 genes represented in the formal-colocalization set. Such a restricted enrichment analysis was not performed in the present study.

Another important observation is the highly modular structure of immune-genetic regulation across metabolic traits. Functional enrichment and PPI analyses demonstrated coordinated biological programs involving antigen presentation, cytokine signaling, mitochondrial pathways, translational regulation, and lipid metabolism. These findings indicate that immune-mediated metabolic dysfunction is unlikely to be driven by isolated genes alone, but instead reflects interconnected immunometabolic networks operating across multiple cellular contexts. Notably, several prioritized genes exhibited extensive cross-trait pleiotropy, suggesting shared upstream regulatory mechanisms linking obesity, dyslipidemia, inflammation, and vascular-metabolic dysfunction. Such convergence may partly explain why MetS frequently clusters with cardiovascular disease, NAFLD, and insulin resistance within the broader cardiometabolic continuum.

Among all prioritized genes, *FADS1* was selected for further investigation as a Tier 1 candidate, although *HSPA1L* had the highest composite priority score. Interpretation of the *FADS1* signal requires particular caution because *FADS1*, *FADS2*, and *FADS3* are located within a linked region on chromosome 11. A cis-eQTL annotated to *FADS1* may tag regulatory variation affecting neighboring genes or metabolic pathways outside the profiled immune cell[23]. Moreover, 40,849 of 42,257 primary MR tests (96.7%) relied on a single-instrument Wald ratio, which does not permit a reliable assessment of horizontal pleiotropy. Colocalization and SMR/HEIDI provide complementary evidence about regional signal sharing, but neither uniquely identifies *FADS1* as the effector gene or monocytes as the causal cell type. We therefore regard *FADS1* as a candidate for locus-level follow-up rather than an established mediator of MetS. *FADS1* encodes the rate-limiting Δ5-desaturase responsible for endogenous PUFA remodeling and conversion of dihomo-γ-linolenic acid (DGLA) to arachidonic acid (AA), thereby influencing downstream lipid mediator synthesis and inflammatory signaling[24]. Previous studies have linked *FADS1* variants to circulating lipid profiles, inflammatory phenotypes, obesity, and cardiovascular risk[25,26].

Our analyses place the genetic prioritization of *FADS1* in the context of expression data from immune cells, adipose tissue, and liver. However, the disease-associated expression findings varied across cohorts and clinical subgroups. In GSE159924, hepatic *FADS1* expression did not differ significantly between obese participants without NAFLD and lean participants, whereas lower expression was observed in obese participants with NAFLD. In GSE126848, expression was significantly lower in the obese, NAFLD, and NASH groups than in normal controls. Together with the adipose-tissue findings, these observations raise the possibility of context-dependent *FADS1* regulation. However, differences in cohort composition, tissue sampling, and analytical methods may also contribute to the observed patterns. Because these analyses used independent cross-sectional datasets, they do not establish a consistent opposite-direction expression pattern between immune cells and metabolic tissues or changes occurring during disease progression. Cell-type-resolved perturbation experiments combined with lipid-species measurements and desaturase-activity assays will be required to clarify the functional relevance of these observations.

A particularly important aspect of this study is the integration of nutrigenetic and population-level cardiometabolic analyses. Emerging evidence suggests that dietary PUFA exposure modifies the metabolic effects of *FADS1* genetic variation, supporting the concept of diet-gene interaction in cardiometabolic disease[27,28]. The NHANES analyses further support this context-dependent interpretation. Higher serum log(AA/DGLA) proxy of delta-5 desaturase activity, reflected by a higher serum log(AA/DGLA) ratio, was associated with lower adiposity, reduced triglycerides and TG/HDL-C ratio, higher HDL-C, lower diastolic blood pressure, and reduced systemic inflammatory markers. These findings suggest that preserved systemic PUFA remodeling capacity is linked to a more favorable cardiometabolic profile. Importantly, this does not imply that increased FADS1 activity is uniformly protective in all tissues. Rather, systemic fatty acid ratios may capture whole-body lipid remodeling efficiency, whereas tissue-specific *FADS1* expression may reflect local adaptive or maladaptive responses to metabolic stress. This distinction helps reconcile the increased *FADS1* expression observed in immune cells with the favorable systemic phenotype associated with higher serum log(AA/DGLA) proxy of delta-5 desaturase activity.

From a translational perspective, our study highlights *FADS1* as a potential target for precision nutritional and immunometabolic intervention. Because *FADS1*-mediated lipid remodeling is strongly influenced by dietary fatty acid exposure, modulation of PUFA intake may represent a biologically plausible strategy for modifying downstream inflammatory and cardiometabolic risk pathways. Importantly, the observed compartment-specific divergence suggests that therapeutic strategies targeting *FADS1* may require tissue-aware or context-dependent approaches rather than uniform systemic activation or inhibition. More broadly, our integrative analytical framework may facilitate the identification of additional immune-derived therapeutic and nutrigenetic regulators across other cardiometabolic and inflammatory diseases.

Several limitations should be acknowledged. First, our analyses focused on circulating immune-cell populations and may not capture tissue-resident immune cells in adipose, liver, or vascular tissues. Most primary MR estimates relied on a single instrument, limiting our ability to assess horizontal pleiotropy with multi-instrument sensitivity methods. Although Steiger tests favored the specified exposure-to-outcome orientation for all primary tests, this was expected in part because the strong cis-eQTL instruments generally explained more variance in gene expression than in the metabolic outcomes. Steiger results therefore served as a consistency check and did not establish causal direction or exclude pleiotropy. The observed effect sizes were modest [approximately odds ratios (ORs) 1.01-1.16 per genetically proxied standard-deviation increase in gene expression] and should be interpreted as population-level relative associations rather than individual-level risk-prediction estimates or expected effects of a therapeutic intervention. Small effects may nevertheless be biologically relevant when aggregated across multiple loci, pathways, or lifelong genetic exposure.

The FADS locus presents a further gene-attribution limitation. Linked variants may regulate *FADS1*, *FADS2*, or *FADS3*, and the instruments may affect metabolic outcomes through circulating lipids or other pathways. An eQTL detected in monocytes may also reflect regulation shared with other immune cells or metabolic tissues. Thus, the analyses cannot identify the effector gene or mediating cell type without further conditional analyses and experimental perturbation. The 192-gene ranking partly relied on associations retained by an exploratory LD-based screen without formal colocalization support; its Tier assignments are therefore intended for follow-up prioritization, not causal-gene classification. Finally, the nutrigenetic synthesis and cross-sectional NHANES analyses do not establish a *FADS1*-mediated lipid mechanism and remain susceptible to residual confounding.

An additional limitation is that the discovery immune-cell eQTL data and the outcome GWAS datasets were derived predominantly from European-ancestry populations. Therefore, the generalizability of these findings to other ancestry groups remains uncertain. In addition, the three metabolic-syndrome-related outcomes

analyzed in this study represent correlated phenotype definitions and should not be interpreted as three independent replication datasets. Concordance across these outcomes may reflect shared phenotype structure and genetic correlation rather than independent validation.

Conclusions

In conclusion, this study maps immune-cell-resolved genetic associations with MetS and related traits and identifies *FADS1* as a candidate gene for further investigation. The genetic, transcriptomic, and cross-sectional fatty acid findings provide complementary but distinct forms of evidence. They do not establish *FADS1*-specific enzymatic activity, the causal cell or tissue, or the effects of modulating *FADS1*. Experimental perturbation and direct lipidomic measurements are needed to test whether and how the FADS locus contributes to metabolic disease.

DECLARATIONS

Acknowledgments

We thank the investigators and participants of the publicly available GWAS, single-cell cis-eQTL, GEO, and NHANES datasets used in this study for making these valuable resources accessible to the scientific community.

Authors' contributions

Conceptualized the study: Sun Y, Liu F, Wang C

Performed data curation and statistical analyses: Sun Y, Zhang X, Zhang F, Li S, Wang X, Liu F, Wei H, Sun Q, Zhang Z

Supervised the analytical workflow and interpretation of the results: Sun Y, Zhang X, Hou X, Wang C

Contributed to the interpretation of the genetic association findings and critically revised the discussion of the evidence supporting *FADS1* as a candidate locus in MetS: Yang T

Contributed to the biological interpretation of the immune cell-specific findings and critically revised the corresponding sections of the Discussion: Wang L

Drafted the manuscript: Sun Y

Revised the manuscript for important intellectual content: Sun Y, Liu F, Hou X, Wang C, Yang T, Wang L

All authors participated in data interpretation, discussed the results, and approved the final version of the manuscript.

Availability of data and materials

All datasets analyzed in this study are publicly available. Single-cell immune cell cis-eQTL summary statistics and GWAS summary datasets used for MR analyses were obtained from publicly accessible repositories as described in the Methods section. Public transcriptomic datasets used for cross-tissue validation and metabolic disease analyses were downloaded from the Gene Expression Omnibus (GEO) database, including GSE200744, GSE32575, GSE196387, GSE159924, GSE126848, GSE141432, and GSE24883. Bulk tissue expression data from the Genotype-Tissue Expression (GTEx) project and immune cell expression data from the Human Protein Atlas (HPA) database were additionally used for tissue- and immune-cell-specific expression profiling. Data from the metabolically healthy *vs.* unhealthy obesity (MHUO) cohort were obtained from the Wolfrum Lab repository (https://github.com/WolfrumLab/MHUO/). NHANES 2013-2014 data used for nutrigenetic and population-level cardiometabolic analyses are publicly available through the Centers for Disease Control and Prevention (CDC) NHANES database. Processed data and analysis scripts generated during this study are available from the corresponding author upon reasonable request.

AI and AI-assisted tools statement

During the preparation of this manuscript, the AI tool OpenAI ChatGPT (version GPT-5.5, accessed on November 10, 2026) was used solely for language editing, and the AI tool OpenAI image-generation tool was used solely to assist in preparing the Graphical Abstract. In addition, the AI tool OpenAI Codex was used

solely to prepare Figure 8A and B, which were subsequently assembled and edited in Adobe Illustrator. These tools did not influence the study design, data collection, analysis, interpretation, or the scientific content of the work. All authors take full responsibility for the accuracy, integrity, and final content of the manuscript.

Financial support and sponsorship

This study was supported by the National Key Research and Development Program of China (grant number 2022YFA1004801).

Conflicts of interest

All authors declared that there are no conflicts of interest.

Ethical approval and consent to participate

This study was based exclusively on publicly available summary-level datasets and de-identified public databases, including GWAS, GEO, GTEx, Human Protein Atlas, and NHANES resources. No new human participants were recruited and no additional human specimens were collected for this study. The original studies from which these datasets were derived obtained the relevant ethical approvals and informed consent. Therefore, no additional ethical approval or informed consent was required for the present secondary analysis.

Consent for publication

Not applicable.

Copyright

© The Author(s) 2026.

Supplementary Materials

Supplementary Materials

REFERENCES

1. Dhondge RH, Agrawal S, Patil R, Kadu A, Kothari M. A comprehensive review of metabolic syndrome and its role in cardiovascular disease and type 2 diabetes mellitus: mechanisms, risk factors, and management. *Cureus* 2024;16:e67428. DOI PubMed PMC
2. Hamooya BM, Siame L, Muchaili L, Masenga SK, Kirabo A. Metabolic syndrome: epidemiology, mechanisms, and current therapeutic approaches. *Front Nutr* 2025;12:1661603. DOI PubMed PMC
3. van de Vyver M. Immunology of chronic low-grade inflammation: relationship with metabolic function. *J Endocrinol* 2023;257:e220271. DOI PubMed
4. Islam MS, Wei P, Suzauddula M, et al. The interplay of factors in metabolic syndrome: understanding its roots and complexity. *Mol Med* 2024;30:279. DOI PubMed PMC
5. Shaikh SR, Beck MA, Alwarawrah Y, MacIver NJ. Emerging mechanisms of obesity-associated immune dysfunction. *Nat Rev Endocrinol* 2024;20:136-48. DOI PubMed PMC
6. Wang X, Chen L, Wei J, et al. The immune system in cardiovascular diseases: from basic mechanisms to therapeutic implications. *Signal Transduct Target Ther* 2025;10:166. DOI PubMed PMC
7. Yazar S, Alquicira-Hernandez J, Wing K, et al. Single-cell eQTL mapping identifies cell type-specific genetic control of autoimmune disease. *Science* 2022;376:eabf3041. DOI PubMed
8. Wang S, Liu S, Zhang H, et al. Integrative functional genomics and fine-mapping identify regulatory mechanisms of multivariate obesity GWAS and its cardiometabolic implications. *Metabolism* 2026;177:156509. DOI PubMed
9. Chami N, Wang Z, Svenstrup V, et al. Genetic subtyping of obesity reveals biological insights into the uncoupling of adiposity from its cardiometabolic comorbidities. *Nat Med* 2025;31:3801-12. DOI PubMed PMC
10. Nathan A, Asgari S, Ishigaki K, et al. Single-cell eQTL models reveal dynamic T cell state dependence of disease loci. *Nature* 2022;606:120-8. DOI PubMed PMC
11. Kim-Hellmuth S, Aguet F, Oliva M, et al. ; GTEx Consortium. Cell type-specific genetic regulation of gene expression across human tissues. *Science* 2020;369:eaaz8528. DOI
12. Kang JB, Raveane A, Nathan A, Soranzo N, Raychaudhuri S. Methods and insights from single-cell expression quantitative trait loci. *Annu Rev Genomics Hum Genet* 2023;24:277-303. DOI PubMed PMC

13. Gittess D, Thompson I, Traktuev DO, Duarte JD, Keeley EC. Fatty acid desaturase genetic variations in heart failure and cardiovascular disease. *Am Heart J Plus* 2025;53:100529. DOI PubMed PMC
14. Batista LD, Rogero MM, Sarti FM, et al. FADS1 and FADS2 gene polymorphisms affect omega-3 and omega-6 erythrocyte fatty acid composition and influence the association between dietary fatty acid intake and lipid profile in brazilian adults. *Metabolites* 2025;15:758. DOI PubMed PMC
15. Sergeant S, Keith BA, Seeds MC, et al. Impact of FADS gene variation and dietary fatty acid exposure on biochemical and anthropomorphic phenotypes in a Hispanic/Latino cohort. *Front Nutr* 2023;10:1111624. DOI PubMed PMC
16. Hellstrand S, Sonestedt E, Ericson U, et al. Intake levels of dietary long-chain PUFAs modify the association between genetic variation in FADS and LDL-C. *J Lipid Res* 2012;53:1183-9. DOI PubMed PMC
17. Dumont J, Goumidi L, Grenier-Boley B, et al. Dietary linoleic acid interacts with FADS1 genetic variability to modulate HDL-cholesterol and obesity-related traits. *Clin Nutr* 2018;37:1683-9. DOI PubMed
18. Park S, Kim DS, Kang S. Carrying minor allele of FADS1 and haplotype of FADS1 and FADS2 increased the risk of metabolic syndrome and moderate but not low fat diets lowered the risk in two Korean cohorts. *Eur J Nutr* 2019;58:831-42. DOI PubMed
19. Lankinen MA, de Mello VD, Meuronen T, et al. The FADS1 genotype modifies metabolic responses to the linoleic acid and alpha-linolenic acid containing plant oils-genotype based randomized trial FADSDIET2. *Mol Nutr Food Res* 2021;65:e2001004. DOI PubMed
20. Meuronen T, Lankinen MA, Kärkkäinen O, et al. FADS1 rs174550 genotype and high linoleic acid diet modify plasma PUFA phospholipids in a dietary intervention study. *Eur J Nutr* 2022;61:1109-20. DOI PubMed PMC
21. Vaittinen M, Lankinen MA, Käkelä P, et al. The FADS1 genotypes modify the effect of linoleic acid-enriched diet on adipose tissue inflammation via pro-inflammatory eicosanoid metabolism. *Eur J Nutr* 2022;61:3707-18. DOI PubMed
22. GTEx Consortium. The GTEx Consortium atlas of genetic regulatory effects across human tissues. *Science* 2020;369:1318-30. DOI PubMed PMC
23. Coulson M, Mutch DM. Molecular insights into the functional roles of variants in the FADS gene cluster on omega-3 long-chain polyunsaturated fatty acid synthesis. *Lifestyle Genom* 2026;19:9-22. DOI PubMed PMC
24. Gromovsky AD, Schugar RC, Brown AL, et al. Δ-5 fatty acid desaturase FADS1 impacts metabolic disease by balancing proinflammatory and proresolving lipid mediators. *Arterioscler Thromb Vasc Biol* 2018;38:218-31. DOI PubMed PMC
25. Yuan S, Bäck M, Bruzelius M, Mason AM, Burgess S, Larsson S. Plasma phospholipid fatty acids, FADS1 and risk of 15 cardiovascular diseases: a Mendelian randomisation study. *Nutrients* 2019;11:3001. DOI PubMed PMC
26. Wang Y. Mendelian randomization identifies causal effects of phospholipids on portal vein thrombosis risk: FADS1/2-mediated pathways and their potential as diagnostic biomarkers. *Nutr Metab* 2026;23:26. DOI PubMed PMC
27. Visioli F, Alfredo Martínez J, Tomé-Carneiro J. Genetic modulation of omega-3 and omega-6 polyunsaturated fatty acid metabolism and health outcomes: a systematic review. *Food Funct* 2026;17:2176-91. DOI PubMed
28. Wu JHY, Micha R, Mozaffarian D. Dietary fats and cardiometabolic disease: mechanisms and effects on risk factors and outcomes. *Nat Rev Cardiol* 2019;16:581-601. DOI PubMed

Disclaimer/Publisher's Note: All statements, opinions, and data contained in this publication are solely those of the individual author(s) and contributor(s) and do not necessarily reflect those of OAE and/or the editor(s). OAE and/or the editor(s) disclaim any responsibility for harm to persons or property resulting from the use of any ideas, methods, instructions, or products mentioned in the content.

© The Author(s) 2026. Open Access This article is licensed under a Creative Commons Attribution 4.0 International License (https://creativecommons.org/licenses/by/4.0/), which permits unrestricted use, sharing, adaptation, distribution and reproduction in any medium or format, for any purpose, even commercially, as long as you give appropriate credit to the original author(s) and the source, provide a link to the Creative Commons license, and indicate if changes were made.